Geochemistry, Geophysics, Geosystems

RESEARCH ARTICLE
10.1029/2017GC007411

Special Section:
The Arctic: An AGU Joint Special Collection

Sediment Provenance Changes in the Western Arctic Ocean in Response to Ice Rafting, Sea Level, and Oceanic Circulation Variations Since the Last Deglaciation

Charles-Edouard Deschamps[1,2,3], **Jean-Carlos Montero-Serrano**[1,2,3], **and Guillaume St-Onge**[1,2,3]

[1]Institut des sciences de la mer de Rimouski, Université du Québec à Rimouski, Rimouski, Québec, Canada, [2]Canada Research Chair in Marine Geology, Institut des sciences de la mer de Rimouski, Université du Québec à Rimouski, Rimouski, Québec, Canada, [3]GEOTOP Research Center, Montréal, Québec, Canada

Abstract Two sediment piston cores were recovered from the Chukchi-Alaskan (05JPC) and Canadian Beaufort (02PC) margins to investigate grain-size, geochemical, and mineralogical compositions. This allowed the reconstruction of changes in detrital sediment provenance and transport related to climate variability since the last deglaciation. The end-member modeling analyses of grain size indicate that sea ice and nepheloid transport and the Mackenzie River sediment plume are major factors influencing sedimentation in the Chukchi-Alaskan and Canadian Beaufort margins, respectively. Unmixing of the sediment composition indicates that detrital sediments in core 02PC are derived mainly from the Mackenzie River, whereas sediments from core 05JPC are derived mainly from the Mackenzie River during the deglaciation and include a mixture of Holocene sediments from the Bering Strait, Mackenzie River, and Eurasian margin. The dolomite-rich ice-rafted debris recorded in both cores could be related to the different phases of iceberg discharges from the Amundsen Gulf Ice Stream. Quartz and feldspar-rich ice-rafted debris dated at 13 and 10.6 ka cal BP (before present) are related to the Lake Agassiz outburst in core 02PC and meltwater discharge from the Brooks Range glaciers in core 05JPC. Detrital proxies in core 02PC support the hypothesis that large meltwater and iceberg discharges from the Lake Agassiz outburst to the Arctic Ocean and Amundsen Gulf ice stream may have triggered the Younger Dryas. Finally, similar trends observed between sea level curves and our detrital proxy suggest that the sea level changes in the western Arctic Ocean have an important influence on the sediment dynamic during the early to middle Holocene.

Key Points:
- Study coupling grain-size, geochemical, and mineralogical proxies in the Chukchi-Alaskan and Canadian Beaufort margins
- The dolomite-rich ice-rafted debris layers in both the Chukchi and Beaufort margins originate from the Amundsen Gulf Ice Stream
- Lake Agassiz outburst flood evidence at the beginning of the Younger Dryas in the Canadian Beaufort margin

Supporting Information:
- Supporting Information S1

Correspondence to:
C.-E. Deschamps,
deschampscharlesedouard@gmail.com

Citation:
Deschamps, C.-E., Montero-Serrano, J.-C., & St-Onge, G. (2018). Sediment provenance changes in the western Arctic Ocean in response to ice rafting, sea level, and oceanic circulation variations since the last deglaciation. *Geochemistry, Geophysics, Geosystems*, *19*, 2147–2165. https://doi.org/10.1029/2017GC007411

Received 26 DEC 2017
Accepted 11 MAY 2018
Accepted article online 7 JUN 2018
Published online 20 JUL 2018
Corrected 15 AUG 2018

This article was corrected on 15 AUG 2018. See the end of the full text for details.

1. Introduction

Sedimentation in the Arctic Ocean and marginal seas has many peculiar characteristics related to the dominance of terrigenous input, which is derived mainly from the surrounding continents with different mineral assemblages and geochemical signatures (Darby et al., 2011; Fagel et al., 2014; Maccali et al., 2013; Vogt, 1997). This land-derived terrigenous material originated from a cold climate under conditions of minimal chemical weathering and therefore consists of weakly altered detrital particles from the original source rocks. This allows correlation between the mineralogical and geochemical signatures preserved in the Arctic shelf sediments and the petrographic composition of the surrounding continents (Gamboa et al., 2017). Detrital sediments are delivered into the Arctic Ocean mainly as suspended particulate matter and bed loads from several large river systems including the Mackenzie, Yukon, Kolyma, Lena, Ob, and Yenisei Rivers (Wagner et al., 2011), as well as from coastal erosion (Gamboa et al., 2017). In shallow continental margins, suspended terrigenous particles are further dispersed by ocean currents and/or incorporated into the sea ice during formation and are then transported over long distances by the surface currents throughout the Arctic Ocean, finally settling far from their source of origin (Darby et al., 2012).

Under this framework, a number of studies have characterized and compiled the regional mineralogical and geochemical compositions of the detrital sediments over the continental shelf from the Eurasian Basin (Schoster et al., 2000; Viscosi-Shirley, Mammone, et al., 2003; Viscosi-Shirley, Pisias, & Mammone, 2003; Vogt, 1997), Chukchi Sea-Bering Strait (Kobayashi et al., 2016; Stein et al., 2017), Chukchi-Alaskan margin (Darby et al., 2012; Naidu et al., 1982; Naidu & Mowatt, 1983; Ortiz et al., 2009; Yamamoto et al., 2017), Canadian Beaufort Shelf, and Amundsen Gulf (Gamboa et al., 2017; Naidu et al., 1971). These data sets allow characterizing the regional surface sediment patterns of the mineralogical and geochemical compositions related to the main sediment sources in the circum-Arctic region. Once this first crucial step has been

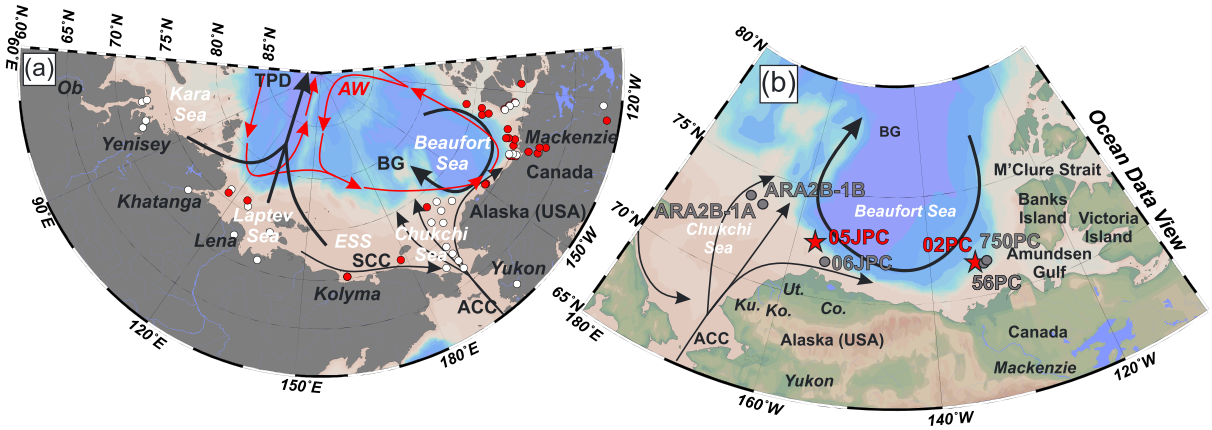

Figure 1. (a) Schematic map of Arctic oceanic circulation and localization of the mineralogical (red circle) and geochemical (white circle) database. (b) Localization of cores 05JPC and 02PC (this study) as well as cores 56PC (Lakeman et al., 2018), 750PC (Scott et al., 2009), ARA2B-A1 (Yamamoto et al., 2017), ARA2B-1B (Stein et al., 2017), and core 06JPC (Ortiz et al., 2009). References used for the geochemical and mineralogical database are listed in Table S2 (mineralogical data: Andrews et al., 2016; Belt et al., 2010; Darby et al., 2011; Gamboa et al., 2017; Gamboa, 2017; Lakeman et al., 2018; Stein et al., 2017; geochemical data: Astakhov et al., 2013; Gamboa et al., 2017; Gordeev et al., 2007; Holemann et al., 1999; Rachold, 1999; Rachold et al., 1996; Savenko et al., 2004). BG = Beaufort Gyre; TPD = Transpolar Drift.

achieved, it is possible to use the mineralogical and geochemical signatures preserved in the Arctic Ocean sedimentary records to reconstruct and better interpret the past variations in sediment inputs, as well as the transport pathways related to late Quaternary climate and oceanographic changes. However, most of the bulk mineralogical records that have been generated do not quantify the contribution of possible sediment sources in the western Arctic Ocean nor their long-term variability. On the other hand, the high sedimentation rates observed in the postglacial sedimentary sequences from the continental margins of the Canadian Beaufort (~10–60 cm/ka; Deschamps et al., 2017) and Chukchi (~30–300 cm/ka; Barletta et al., 2008; Lisé-Pronovost et al., 2009) Seas in Arctic Ocean offer records for reconstructing sediment dynamics and past climate conditions at the centennial to millennial time scales.

In this regard, in the present study, grain-size, mineralogical, and elemental geochemical analyses of the bulk (<2 mm) and clay (<2 μm) sediment fractions were carried out on two sediment piston cores recovered from the Chukchi-Alaskan (core HLY01-05JPC) and Canadian Beaufort (core AMD0214-02PC) margins in order to (1) assess the contributions from specific sediment sources (e.g., East Siberian Sea, Kara Sea, Northwest Alaska, Mackenzie River, Bering Strait inflow, and Canadian Arctic Archipelago) and (2) provide new insights on potential relations between ice rafting, sea level, and oceanic circulation variations and sediment dynamics in the western Arctic Ocean since the last deglaciation. Thus, our study differs from these earlier publications in terms of methodological approach (quantitative mineralogy and multiproxy study), intermargin comparison (Chukchi-Alaskan versus Canadian Beaufort margins), and enhanced discrimination of circum-Arctic sediment sources. Therefore, this multiproxy record provides an opportunity to reconstruct sediment dynamics within the western Arctic Ocean since the deglaciation.

2. Regional Setting

2.1. Oceanic Circulation

The Arctic surface oceanic circulation is related to two main, wind-driven circulation systems, which are the anticyclonic Beaufort Gyre (BG) in the western Arctic and the Transpolar Drift (Darby & Bischof, 2004; Tremblay et al., 1997). At a regional level, these surface circulation regimes are controlled mainly by changes in the phase of large-scale atmospheric patterns, such as the Arctic Oscillation (AO; Darby & Bischof, 2004; Darby et al., 2012) and the Pacific Decadal Oscillation (Overland et al., 1999), which are both significant natural patterns in global climate variability. On the other hand, the Chukchi shelf circulation is controlled by an inflow of Pacific waters via the Bering Strait (referred to as the Bering Strait inflow), the Siberian coastal current, and the Atlantic Intermediate Water affecting the northern margin (Pickart, 2004; Weingartner et al., 2005). The Pacific inflow can be divided into three major branches (Figure 1). The first branch turns westward around Herald Canyon. The third branch flows into Barrow Canyon, whereas the second branch flows between the first and the third branches (Weingartner et al., 2005). The Bering Strait inflows are controlled

mainly by the Aleutian Low strength and position at the interannual time scales (Yamamoto et al., 2017). Indeed, periods of strengthening of the Aleutian Low pressure center, located over the eastern North Pacific, induce an increase of the Bering Strait inflow into the Arctic Ocean (Danielson et al., 2014). On the Canadian Beaufort shelf, the anticyclonic BG pushes both surface currents and sea ice westward at the shelf break. Conversely, closer to shore around the 50-m isobath, the Beaufort Undercurrent transports both Pacific and Atlantic waters eastward along the continental margin and into the Amundsen Gulf (Forest et al., 2011).

2.2. Surrounding Geology

Because the Arctic Ocean is a semi-enclosed basin, detrital sediment source regions for the Arctic are limited to the surrounding terrains: the Canadian Arctic Archipelago, the Mackenzie delta region, Northern Alaska, the Chukchi Sea with Pacific influences, the East Siberian Sea, the Laptev Sea, the Kara Sea, the Barents Sea, and the Pan-African terrains of Northern Greenland (Fagel et al., 2014). These circum-Arctic sources areas have variable geological ages and tectonic settings and are therefore characterized by different petrographic signatures. The Canadian Arctic Archipelago and the Mackenzie Delta region comprise shales and sandstones from marine and nonmarine sedimentary rocks (Harrison et al., 2011). In addition, Banks and Victoria Islands are composed of shale and sandstones rich in dolomite clasts, as well as quartz and feldspar grains (Bischof & Darby, 1999; Dong et al., 2017; Phillips & Grantz, 2001). As part of the North American margin, the Canadian Shield is made of Archean plutonic and metamorphic rocks (Padgham & Fyson, 1992). Alaskan terrains include Canadian-Alaskan Cordillera, Brooks Range, and part of the North American platform containing mostly metamorphic and clastic rocks (Hamilton, 1986). The Siberian platform is composed of Precambrian and Cambrian limestones, Jurassic to Cretaceous terrigenous sediments and Quaternary alluvial material (Harrison et al., 2011). The volcanic areas can be separate in different zones: the intraplate Okhtosk-Chukotka composed by acidic to intermediate rocks predominating in the west and intermediate to basic rocks in the east (Viscosi-Shirley, Mammone, et al., 2003), as well as the Bering Sea Basalt Province, and the Permian and Triassic volcanic rocks of the Siberian traps, and the convergent margins of the Pacific Aleutian (Gardner et al., 1980; Harrison et al., 2011).

2.3. Sedimentation

On the Canadian Beaufort shelf, most of the surficial seabed sediments are predominantly composed of Holocene marine olive gray silts and clays (Gamboa et al., 2017). Surface sediments from the Chukchi Sea are composed of bioturbated gray to clayey silts (Kobayashi et al., 2016). Modern sedimentation in the Chukchi Sea is believed to be mainly derived from northeastern Siberia, Bering Strait inflow (especially from the Yukon River) and Mackenzie River, whereas the Canadian Beaufort margin sediment originates primarily from the Mackenzie River basin (Darby et al., 2011; Gamboa et al., 2017; Kobayashi et al., 2016). Smaller Alaskan rivers have a more local impact, but may have been a more important sediment source at the early stages of the last transgression (Hill & Driscoll, 2008). During deglaciation and the early Holocene, sediment inputs to the Chukchi and Beaufort margins were presumably higher due to the rising sea level associated with meltwater and iceberg discharge from the retreat of large ice sheets (Deschamps et al., 2017). During the Holocene or interglacial, sediment redistribution is strongly controlled by bottom currents, while during deglacial/glacial period sea ice and ice-rafted debris (IRD) strongly affected sediment dispersal and deposition (Darby et al., 2009). Several IRDs have been recorded in the sedimentation along the North American margin associated with the calving of the Laurentide and Innuitian Ice Sheets (Darby & Zimmerman, 2008).

3. Materials and Methods

3.1. Samples, Sediment Characteristics, and Chronology

The sediment core HLY0501-05JPC (hereafter referred to as core 05JPC; location: 72°51.618′N, 158°25.26′W) was recovered from the Chukchi-Alaskan margin on board the USCGC Healy as part of the 2005 Healy-Oden Trans-Arctic Expedition (Darby et al., 2005; Figure 1b). Physical and magnetic properties of the sediment core 05JPC have been previously published in Barletta et al. (2008). Core AMD0214-02PC (hereafter referred to as core 02PC; location: 71°22.910′N, 133°34.040′W) was collected on the Canadian Beaufort margin on board the CCGS Amundsen during the 2014 ArcticNet expedition (Montero-Serrano et al., 2014; Figure 1b). The age model, magnetic and physical properties of the sediment core 02PC have been described in Deschamps et al. (2017). Note that cores 05JPC and 02PC were raised from the continental slope at 415- and 998-m depth, respectively, where sediment deposition was not interrupted by sea level changes. The sediment core 02PC was sampled evenly every 10 cm in the Holocene and IRD intervals, as well as every 20 cm in the deglacial

interval for a total of 42 samples. The sediment core 05JPC was sampled every 60 cm in the Holocene interval and every 30 cm for the remaining sections (corresponding to the deglacial interval) for a total of 30 samples.

The sediment cores 05JPC and 02PC present two distinct sedimentary units. According to Barletta et al. (2008), the upper unit in core 05JPC is composed of olive gray mud, and the second unit is characterized by dark gray mud with sandy layers and IRD. Core 02PC consists of homogeneous olive brown to dark gray mud for the upper unit, while the second unit consists of dark gray mud with the presence of white clasts and was interpreted as IRD (Deschamps et al., 2017). The sedimentation rate for core 02PC was lower in the post-glacial parts (10–20 cm/ka) and higher in the glacial parts (60–300 cm/ka). Based on the physical properties and grain-size analyses, the IRD layers were found in the glacial unit in both cores. The IRDs were identified between 1,350 to 1,420 (IRD1A) and 1,560 to 1,620 cm (IRD1B) in core 05JPC (Barletta et al., 2008). Likewise, the IRD in core 02PC consists of white clasts found between 140 and 160 cm (IRD1A), 320 and 350 cm (IRD2A), and 350 and 360 cm (IRD2B). These fine-grained IRDs are generally <63 μm, poorly sorted, have sharp contacts, and consist mainly of rock flour (dolomite and quartz rich). These IRDs are interpreted to reflect enhanced meltwater discharge and iceberg rafting from the Laurentide Ice Sheet (Andrews, 2000; Deschamps et al., 2017; Lakeman et al., 2018; Polyak et al., 2007).

The age model of core 05JPC was constructed using a linear interpolation between the ^{14}C ages for the Holocene and deglacial sections (Barletta et al., 2008) and assuming a $\Delta R = 460$ as suggested in Darby et al. (2009). The best ^{14}C-based age control covers the interval of 2–6.9 ka cal BP in 05JPC. Ages below this dated interval were extrapolated, and our interpretations thus remain hypothetic. However, the very similar paleomagnetic secular variations between core 05JPC and other Arctic records (Barletta et al., 2008) suggest a valid age model around 8.5–9 ka cal BP. Based on this age model, core 05JPC spans the last 11 ka cal BP and IRD1A-B were dated at 9.5 and 10.6 ka cal BP, respectively. In the same way, the age model of core 02PC published in Deschamps et al. (2017) by a bayesian approach (Blaauw & Christen, 2011), was improved using the new ages from the nearby core 56PC presented in Lakeman et al. (2018) and assuming a $\Delta R = 335 \pm 85$ for the Holocene interval and a $\Delta R = 1{,}000$ for the deglacial interval (Coulthard et al., 2010; Hanslik et al., 2010; McNeely et al., 2006). Conventional 14C ages was calibrated with Marine13 (Reimer et al., 2013). Contemporaneous IRD peaks have been identified in magnetic susceptibility curves and used in order to transfer the age model of core 56PC to core 02PC (see the supporting information). Finally, core 02PC spans the last 13.2 ka cal BP and the IRD1A and IRD2A-2B are dated to ~11, 12.8, and 13 ka cal BP, respectively (Figure S1).

3.2. Grain-Size Distribution and End-Member Modeling Analysis

Sediment grain-size analyses were performed on the detrital bulk sediment samples using a Beckman Coulter LS13320 laser diffraction grain-size analyzer following the protocol in Deschamps et al. (2017). The grain-size distribution and statistical parameters (e.g., mean and sorting) were calculated using the moment methods from the GRADISTAT software (Blott & Pye, 2001). The end-member modeling algorithm (EMMA), developed by Weltje (1997) and adapted by Dietze et al. (2012), was applied to the grain-size data in order to extract meaningful end-member (EM) grain-size distributions and estimate their proportional contribution to the sediments. A more detailed description of the EMMA method that we applied can be found in Dietze et al. (2012). Overall, the grain-size loadings, mean grain-size, and EM modeling analyses were used to investigate the sedimentary transfer regime because the sediment grain-size distribution (primarily driven by sedimentary processes) reflects transport conditions (Dietze et al., 2012; Gamboa et al., 2017).

3.3. Geochemical and Mineralogical Analyses

Before geochemical and mineralogical analyses, the sediment samples were rinsed five times with distilled water after the removal of the organic matter fraction with 10 ml of hydrogen peroxide (30% H_2O_2). Next, an aliquot of this sediment sample was used as the bulk fraction (<2 mm), whereas another aliquot was used to separate the clay-sized fraction (<2 μm). A centrifuge-based Atterberg method was used according to Stoke's law to separate the clay-sized fraction. The required settling times were calculated using the software SediCalc (Krumm, 2006). Subsequently, aliquots of the separated bulk and clay-sized samples were oven dried overnight at approximately 60 °C and then slightly homogenized with an agate mortar. These homogenized sediment fractions were used for geochemical and mineralogical analyses.

3.3.1. Bulk Elemental Concentration

A total of 14 elements (Al, Si, K, Mg, Ca, Ti, Mn, Fe, P, Sr, V, Cr, Zn, and Zr) was analyzed on both bulk and clay-sized fractions by energy dispersive X-ray fluorescence spectrometry using a PANalytical Epsilon 3-XL. Before

energy dispersive X-ray fluorescence analysis, samples were treated by borate fusion in an automated fusion furnace (CLAISSE® M4 Fluxer). The analytical procedures were similar to Gamboa et al. (2017). Analytical accuracy and precision were found to be better than 1–5% for major elements and 5–10% for the other elements, as checked against an international standard (U.S. Geological Survey SDC-1) and analysis of replicate samples.

3.3.2. Quantitative Bulk Mineralogy

Bulk mineral associations (<2 mm) were studied by quantitative X-ray diffraction (qXRD) following the method developed by Eberl (2003, 2004) and used in other Quaternary glacial marine studies that address sediment mineralogy (Andrews et al., 2015, 2016; Darby et al., 2011; Stein et al., 2017). For this, ~1 g of each sample was spiked with 0.25 g of corundum and then ground in a McCrone micronizing mill using 5 ml of ethanol to obtain a homogenous powder. The slurry was oven dried overnight at approximately 60 °C and then slightly homogenized with an agate mortar. Next, 0.5 ml of Vertrel was added to the mixture to prevent the possible agglomeration of finer particles. The powder sample is then sieved (<300 μm), back-loaded into the holders and analyzed on a PANalytical X'Pert Powder diffractometer. Samples were scanned from 5° to 65° 2θ in steps of 0.02° 2θ, with a counting time of 4 s per step. For the quantification of the major mineralogical components, sediment X-ray diffraction scans obtained were converted into mineral weight percent (wt. %) using the Excel macro program ROCKJOCK v11 (Eberl, 2003). This program uses a full-pattern fitting method that permits the quantification of whole-sediment mineralogy with a precision of ±3 wt. % (Eberl, 2003). The calculated total mineral weight percent was normalized to a sum of 100%. We focused on 15 key minerals (quartz, K-feldspar, plagioclase, calcite, dolomite, amphibole, Fe-bearing, amorphous silica, kaolinite, chlorite, illite, biotite, muscovite, smectite, and vermiculite) that represented more than 96% of the overall mineral concentration in the bulk sediment sample.

3.3.3. Clay Mineralogy

In this paper, clay minerals were quantified in the bulk sediment fraction (<2 mm) using the Excel macro program RockJock. However, nearly all previous clay mineral provenance studies in the Arctic Ocean used oriented mounts of the <2-μm sediment fraction to identify and semiquantify the clay mineral abundance, notably illite, kaolinite, chlorite, and smectite (Naidu et al., 1971, 1982; Naidu & Mowatt, 1983). Therefore, in this study, the clay-size fraction of all sediment samples was isolated and analyzed in this manner for comparison. Clay minerals were thus studied using X-ray diffraction following established protocols (Bout-Roumazeilles et al., 1999; El Ouahabi et al., 2017). The separated clay-sized fraction (<2 μm) was concentrated by centrifugation and oriented by wet smearing on glass slides. The analyses were run from 2.49° to 32.49° 2θ on a PANalytical X'Pert Powder diffractometer. Three X-ray diagrams were performed, after the sample was air-dried, ethylene glycol vapor saturation was completed for 12 hr, followed by heating at 490 °C for 2 hr. Semiquantitative estimation of clay mineral abundances (smectite, illite, chlorite, kaolinite, vermiculite, and a chlorite/smectite mixed layer) based on peak areas was performed using the MacDiff® 4.2.5 software (Petschick, 2000). Similar to other Arctic clay mineral studies (Schoster et al., 2000; Wahsner et al., 1999), clay mineral contents were calculated by using the weighting factors introduced by Biscaye (1965) and calculated to a sum of 100%. The error on the reproducibility of measurements is estimated to be 5% for each clay mineral, as checked during the analysis of replicate samples. Overall, the combinations of both RockJock and oriented mounted methods are supporting each other and give independent information (e.g., Darby et al., 2011).

3.3.4. Sediment Unmixing Model

We used the nonlinear unmixing Excel macro-program SedUnMixMC (Andrews et al., 2015, 2016; Andrews & Eberl, 2012) to gain a quantitative understanding of the downcore changes in bulk sediment provenance. To avoid misinterpretation of bulk mineralogical results caused by the methodological differences between sources and downcore sediment samples, all sediment source samples used here were processed for qXRD (Andrews et al., 2016; Belt et al., 2010; Darby et al., 2011; Gamboa et al., 2017; Lakeman et al., 2018; Stein et al., 2017; Table S2).

3.3.5. Statistical Approach

The mineralogical and geochemical data are of a compositional nature; that is, they are vectors of non-negative values subjected to a constant-sum constraint (usually 100%). This implies that relevant information is contained in the relative magnitudes, so mineralogical and geochemical data analyses must focus on the ratios between components (Aitchison, 1990). Under this framework, the vertical distributions of the sediment provenance proxies and the discriminant scatter plots based on mineralogical and geochemical data were represented here as log ratios. Note that a log transformation will reduce the very high values and

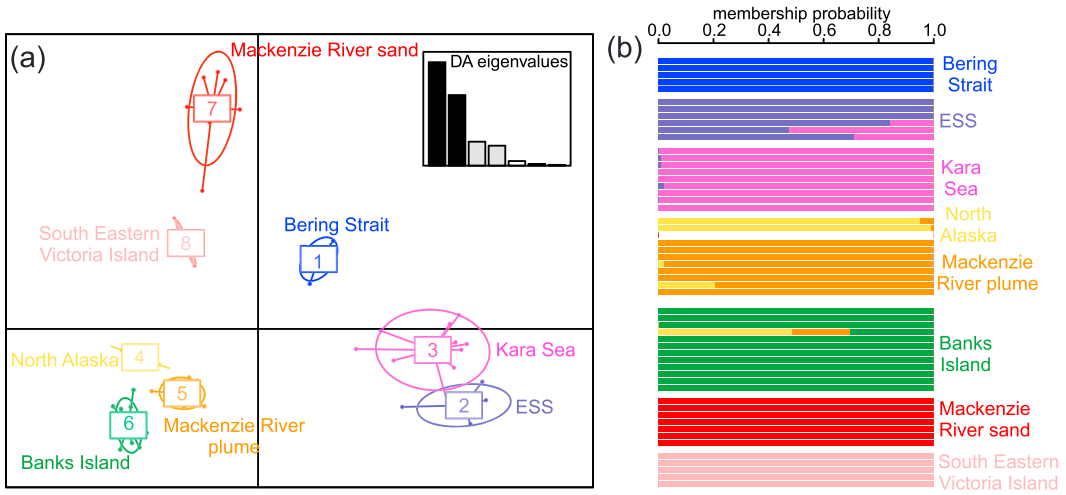

Figure 2. (a) Discriminant function analyses and (b) membership probability of the circum-Arctic sources based on log-ratio mineral data. The membership probability diagram corroborates that potential sediment sources have different mineralogical characteristics that allow a reasonable degree of discrimination, as indicated by their relatively high membership value (up to 90%).

spread out the small data values and is thus well suited for right-skewed distributions (van den Boogaart & Tolosana-Delgado, 2013). Thus, compared to the raw data, the log-ratio scatter plots exhibit better sediment discrimination. In addition, discriminant and membership's probability analyses were performed using the mineralogical data set with the goal of ascertaining whether the differences observed between each sediment source area are statistically valid (Andrews & Vogt, 2014; Figures 2a and 2b). Prior to discriminant and membership's probability analyses, a log-centered (clr) transform was applied to the data set (Aitchison, 1990). Both analyses were conducted with *R* software using the packages *adegenet* (Jombart, 2008) and *compositions* (van den Boogaart & Tolosana-Delgado, 2008).

4. Results and Interpretations

4.1. Grain-Size Distribution and End-Member Modeling

The algorithm of the EM modeling analysis EMMA showed a polymodal distribution and revealed a three-EM model in cores 05JPC and 02PC (Figure 3a). This explains more than 95% of the total variance. The end-member EM3 is associated with medium to coarse silts (10 to 30 μm), end-members EM2 correspond to fine to medium silts (2 to 10 μm), and end-member EM1 is associated with clay to fine silts (0 to 4 μm). Finding the same grain-size EMs in both margins highlights the robustness of the results and suggests that both margins are probably influenced by similar sedimentary processes. The relative contributions of these EMs are plotted against depth in Figure 3b. Darby et al. (2009) have shown the detailed grain-size distribution for sediment transport processes in the western Arctic Ocean using varimax-rotated principal component analysis on several Holocene sediment cores in the Chukchi Sea and including core 05JPC. In their study, they found four main EMs: (i) EM $<$0.5 μm relates to suspension freezing and sediment wash load; (ii) EM centered on 2 μm relates to anchor sea ice; (ii) EM centered on 5 μm is associated with the noncohesive (sortable) fine silt that is commonly transported in suspension by weak currents along the bottom or in nepheloid layers above the bottom; and (iv) specific to the Chukchi margin, EM of 43–64 μm is associated with intermittent suspended load. Overall, these grain-size EM obtained by Darby et al. (2009) are similar to the ones obtain in this study, and therefore, we infer that our grain-size pattern reflects the same sedimentary processes. However, surface sediments derived from the Mackenzie River are also characterized by a fine to medium grain size (4–5 μm; Gamboa et al., 2017), which is similar to the EM centered on 5 μm that is related to nepheloid transport (Darby et al., 2009). Thus, this EM could be interpreted differently between the Chukchi (nepheloid transport) and Canadian Beaufort margins (Mackenzie River sediment plume). Based on these results, the log (EM1/EM2) ratio is used to elucidate downcore variations in the proportion of grains transported by sea ice or nepheloid flow for core 05JPC and by sea ice and/or Mackenzie River discharges for core 02PC.

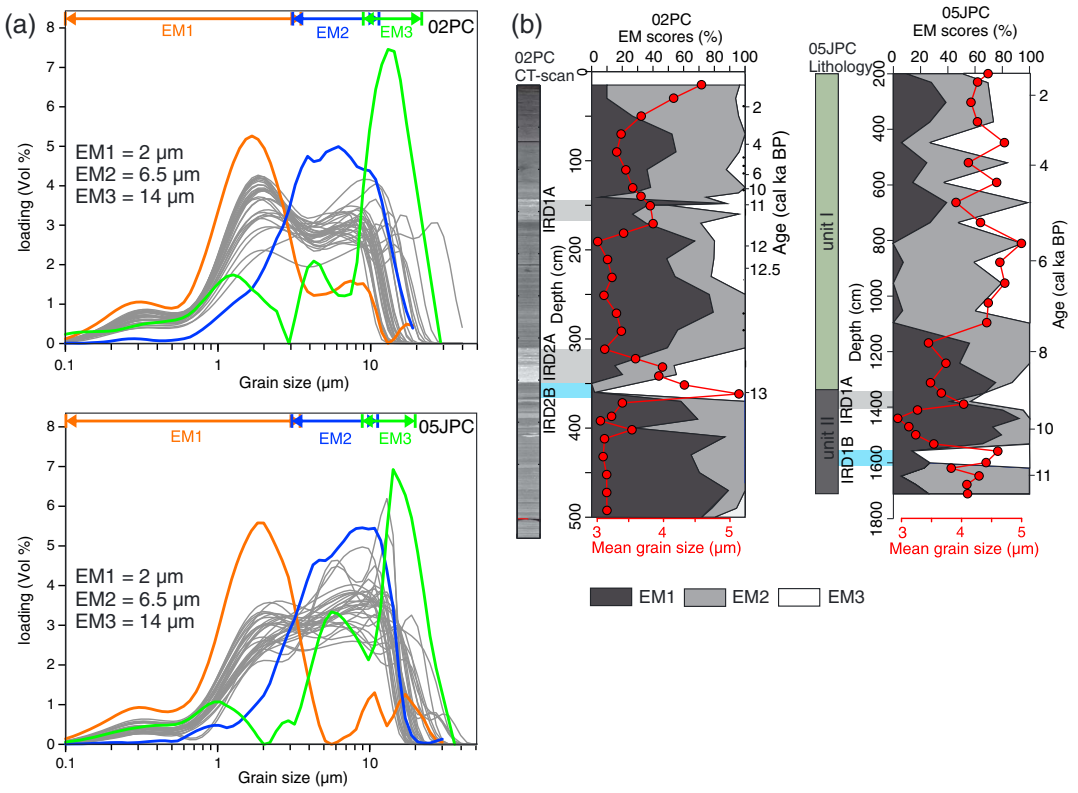

Figure 3. End-member modeling analyses performed on the grain-size distribution of the detrital fraction from cores 01JPC, 05JPC, 03PC, and 02PC. (a) Three representative, unmixed grain-size distributions, and (b) end-member scores (%) derived from end-member modeling analyses are shown. EM = end-member.

4.2. Elemental Geochemistry

Stratigraphic distributions of the elemental geochemical data from the two sedimentary cores studied here are shown in Figure S2. Looking at the variation of the proportion between the different fractions (bulk and clay), we can observe two groups with a different behavior. The first group was related to elements with a higher concentration in the bulk fraction, which included Si, Ti, and Zr, as well as Ca, Mg, and Mn in the IRD intervals. However, note that Ca and Mg in the IRD layers are more enriched in core 02PC than in core 05JPC (maximum values of ~15 and ~3.5 wt. %, respectively). The second group was linked to elements with a higher concentration in the clay fraction, which included Al, K, Fe, V, and Zn for both cores. The downcore variations are quite similar between the bulk and clay fractions in core 02PC. However, some differences in the long-term variations between the bulk and clay fractions are observed in core 05JPC with an increase of Ca, Mg, and Fe in the clay fraction during the early to late Holocene (Figure S3).

Because Al and Si are associated to clay minerals, aluminosilicates, and quartz, and Ca is associated to carbonates, the ternary plot Al, Si, and Ca (expressed as oxides; Figure 4a) was used in order to obtain a general geochemical classification of the sediments (Gamboa et al., 2017). Sediments from cores 05JPC and 02PC are dominantly composed of detrital material, which is similar to an average shale (Pourmand et al., 2012). However, sediments from core 02PC are slightly enriched in Al and depleted in Si in both the bulk and clay fractions compared to core 05JPC. In addition, the clay fraction of core 02PC is also enriched in Al and K, whereas core 05JPC is enriched in Mg and Fe (Figure 4c). Likewise, bulk sediments from cores 02PC and 05JPC have a similar chemical composition to the sediments of the Mackenzie River and Chukchi Shelf/Eurasian Rivers, respectively. In the bulk sediments, the IRD layers showed higher Ca contents (dolomite) and plot along the mixing line from average shale to the detrital carbonate EM (Figure 4a). These Ca-rich IRD layers have a similar composition to the Canadian Arctic Archipelago sediments (including Banks and Victoria Islands; (Belt et al., 2010; Darby et al., 2011; Gamboa et al., 2017).

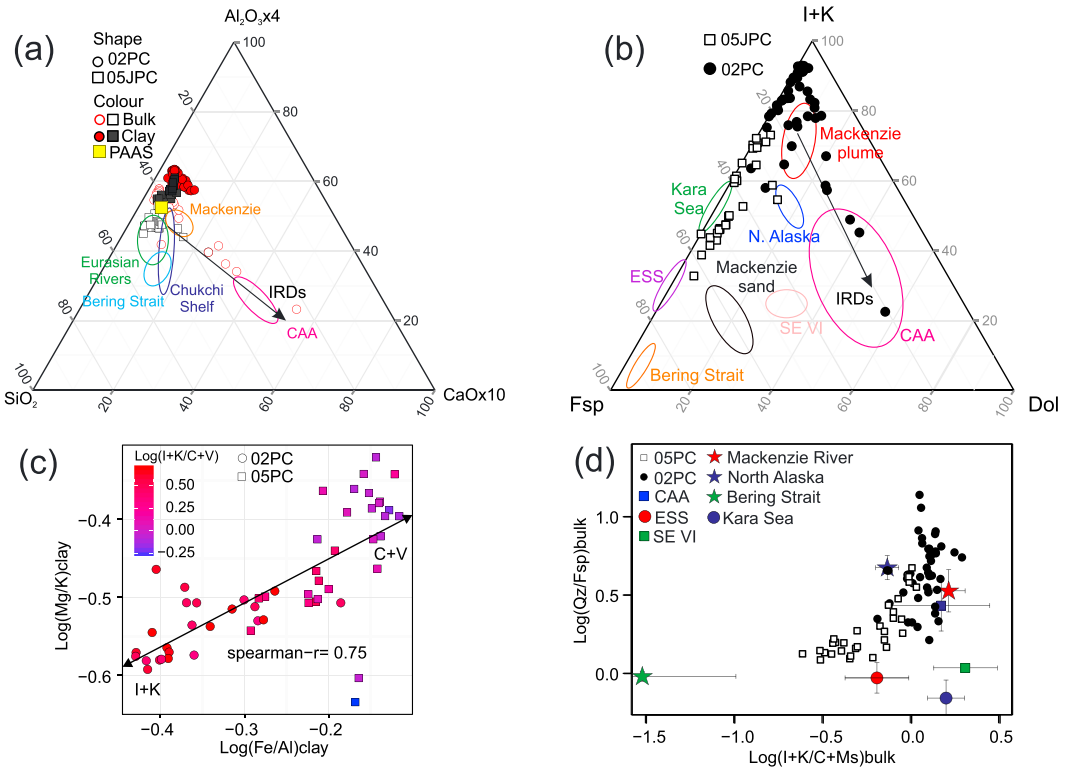

Figure 4. (a) Al_2O_3-SiO_2-CaO ternary plot showing the overall composition (bulk and clay fractions) of the sediment from cores 05JPC and 02PC in comparison to the average shale and circum-Arctic source areas. (b) Kaolinite + Illite (K + I)—total feldspars (Fsp)—dolomite (Dol) ternary plot for cores 05JPC and 02PC based on bulk mineralogy. (c) Relationship between log (Mg/K) and log (Fe/Al) ratios derived from the clay fraction of sediment cores 05JPC (square) and 02PC (circle). The log-ratio I + K/C is represented by a gradient color from high (red) to low (blue) values. (d) Log (Qz/Fsd) versus Log (I + K/Ch + Ms) diagram illustrating the bulk mineralogical difference between cores 02PC and 05JPC and some circum-Arctic regions. Geochemical and mineralogical data of the circum-Arctic regions are shown in Table S2. IRDs = ice-rafted debris.

Based on all the results discussed above, we selected the Log (Ca/Al), Log (Mg/Al), Log (Zr/Al), and log (Fe/Al) ratios to reconstruct downcore changes in sediment provenance and transport on the Chukchi-Alaskan and Canadian Beaufort margins since the last deglaciation (Figures 6 and 7). Indeed, the grain-size changes could be investigated with log (Zr/Al), because Zr is concentrated in zircon grains in the coarser fraction and Al is preferentially associated with clay minerals and aluminosilicates in the fine-grained fractions (von Eynatten et al., 2012). As discussed in Bischof and Darby (1999) and Gamboa et al. (2017), sediments derived from the Canadian Shield, the sedimentary platform along the Mackenzie Valley, and the Western Canadian Arctic Archipelago are characterized by high contents (up to 2%) in iron oxides, including hematite, goethite, pyrite, maghemite, and magnetite. Thus, high log (Fe/Al) ratios could reflect a higher input of iron oxides entrained by icebergs from the Laurentide and Innuitian Ice Sheets (e.g., Bischof & Darby, 1999). In addition, a high Log (Ca/Al) and Log (Mg/Al) ratio may reflect a greater contribution from detrital carbonates (such as dolomite), whereas low ratios may suggest the input of aluminosilicates (Gamboa et al., 2017).

4.3. Bulk Mineralogy

Stratigraphic distributions of the bulk mineralogical data from the two sedimentary cores in this study are shown in Figure S4. The mineralogy of the bulk sediment fraction from the Canadian Beaufort and Chukchi-Alaskan margins is dominated by quartz (02JPC: 13–40%; 05JPC: 12–39%), phyllosilicates, which includes kaolinite, chlorite, illite, biotite, muscovite, smectite, and vermiculite (02JPC: 47–80%; 05JPC: 30–50%), amorphous silica (02PC:0–4.5%; 05JPC:0–25%), plagioclase (02JPC: 1–7%; 05JPC: 4–11%), K-feldspar (02JPC: 0–5%; 05JPC: 1–6%), dolomite (02PC: up to 28%; 05JPC: up to 5%), and lower proportions (<1%) of Fe-bearing, amphibole and pyroxene minerals. In general, quartz, phyllosilicates, plagioclase, and K-feldspar represented more than 80% of the overall mineral concentration in both sediment cores. However, K-

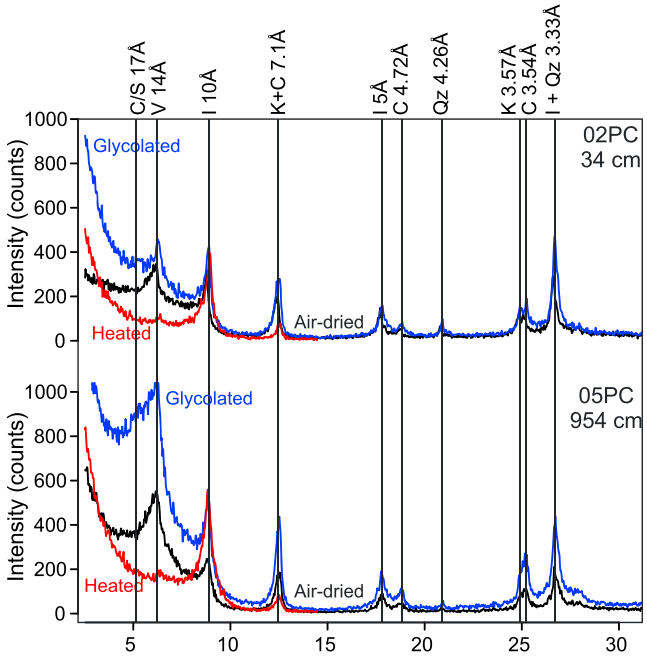

Figure 5. X-ray diffractograms of typical samples from cores 02PC and 05JPC showing interpretation of major clay mineral species from the three classical runs, that is, in air-dried, glycolated, and heated conditions.

feldspar, plagioclase, muscovite, chlorite, and vermiculite are more abundant in core 05JPC, whereas quartz, illite, and kaolinite are enriched in core 02PC (Figures 4c and 4d). In both sediment cores, intervals with punctuated enrichments of dolomite (up to 28% for 02PC and up to 5% for 05JPC) and in quartz (up to 40% in both cores) are observed in the IRD layers (Figure 5). Based on these results, we performed a ternary plot of illite + kaolinite, total feldspars, and dolomite (Figure 4b) to obtain a general mineralogical discrimination of the potential source areas. The Bering Strait and Eurasian sources are characterized by a higher total feldspar proportion, the sediments from the Northern Alaska and Mackenzie River are related to higher illite + kaolinite contents, and the sediments from the Banks and Victoria islands are enriched in dolomite. The sediments of core 02PC are mostly related to the Mackenzie River as potential sources, whereas the sediments of core 05JPC seem to be composed by a mixture of sediments from the Eurasian margin, Bering Strait, and Mackenzie River. The sediments in the IRD layers present higher dolomite contents. Overall, the relative abundance of dolomite and the following ratios are used to trace sediment provenance changes over time: Log [quartz/(K-feldspar + plagioclase)] or Log (Qz/Fsp), Log [phylosillicates/(K-feldspar + plagioclase)] or Log (Phy/Fsp), and Log (illite+kaolinite/chlorite + muscovite) or Log (I + K/C + Ms).

4.4. Clay Mineralogy

Stratigraphic distributions of clay mineralogical data from the two sediment cores studied here are shown in Figure S5. The clay mineral assemblage consists mainly of illite, kaolinite, chlorite, and vermiculite in both cores (Figure 5). Indeed, core 02JPC consists of illite (55–70%), kaolinite (10–30%), chlorite (10–25%), vermiculite (0–20%), and a scarce abundance of a smectite/chlorite mixed layer (0–8%, average, 1%; Figure S5). The clay mineral assemblage for core 05JPC consists of illite (30–70%), chlorite (10–20%), kaolinite (5–15%), vermiculite (5–55%), and smectite/chlorite mixed layer (0–20%), which is present in much less abundance, with average contents of 1% (Figure S5). Thus, as also shown in the bulk qXRD data, the major clay mineralogical difference between the two sediment cores is the higher illite-kaolinite proportion in core 02PC, whereas core 05JPC is relatively enriched in chlorite (see the supporting information). These results are consistent with those reported for modern surface sediments on the Chukchi and Beaufort shelves (Kalinenko, 2001; Krylov et al., 2014; Naidu et al., 1982; Naidu & Mowatt, 1983; Wahsner et al., 1999). Thus, we used the Log (illite + kaolinite/chlorite + vermiculite) ratio or Log (I + K/C + V) to derive changes in transport pathways (e.g., Bering Strait inflow) and the Log (illite/kaolinite) ratio or Log (I/K) to reconstruct changes in sediment inputs within the Canadian Beaufort Shelf.

5. Discussion

Long-term changes in sediment sources were explored using the program SedUnMixMC (Andrews & Eberl, 2012). In core 02PC, we ran SedUnMixMC using surface samples from the following sources: Mackenzie Trough-Canadian Beaufort Shelf, Canadian Arctic Archipelago, Kara Sea, and bed sands from the Mackenzie River basin (Figure 6; see the supporting information). As summarized in Asahara et al. (2012), modern sediment inputs in the Chukchi Sea are mainly derived from northeastern Siberia and Bering Strait inflow and accessorily from the Mackenzie River. Based on this premise, we ran the SedUnMixMC on sediment core 05JPC using the following sediment sources: Bering Strait, Northern Alaska, Eastern Siberian-Laptev Seas, Mackenzie Trough-Canadian Beaufort Shelf, and detrital carbonates from the Canadian Arctic Archipelago, including the Banks/Victoria Islands (Figure 7; see the supporting information). The box plot based on principal component scores of geochemical and mineralogical data (Figure S7; Table S3; Thió-Henestrosa & Martín-Fernández, 2005), ternary plot illite + kaolinite – total feldspars – dolomite (Figure 4b), the Log (Qz/Fsp) – Log (I + K/C + Ms) crossplots (Figure 4d), as well as the discriminant and membership probability analyses based on log-ratio mineral data (Figure 2), indicate that these potential source

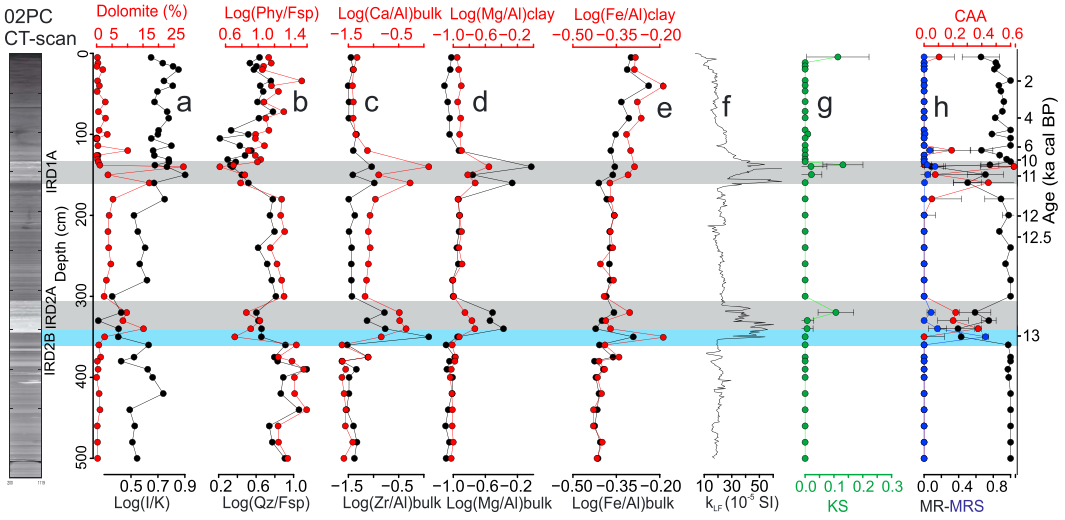

Figure 6. Downcore variations of core 02PC showing (a) log-ratio illite/kaolinite and dolomite content (red). (b) Log-ratios quartz/feldspar (black) and phyllosilicates/feldspar (red). (c) Log-ratio Zr/Al (black) and Ca/Al (red). (d) Log-ratio Mg/Al for the bulk (black) and clay (red) fractions. (e) Log-ratio Fe/Al for the bulk (black) and clay (red) fractions. (f) Magnetic susceptibility, k_{lf} (Deschamps et al., 2017). (g) Proportion of sediment from the Kara Sea (black). (h) Proportion of sediment from the Mackenzie River (black), Mackenzie River sand (blue), and CAA (red). IRD layers rich in dolomite and quartz are highlighted in gray and blue, respectively. IRD = ice-rafted debris.

regions have mineral and chemical compositions that allow a reasonable degree of sediment discrimination as indicated by their relatively high membership value (up to 90%).

In this context, the long-term variations observed in our mineralogical and geochemical records are discussed below in terms of glacial and postglacial changes in detrital sediment supply, provenance, and transport and their possible relations with both the deglacial/Holocene climate variability and relative sea level variations.

5.1. Deglacial/Holocene Sediment Dynamics (14 to 10.5 ka cal BP)

5.1.1. Canadian Beaufort Sea

SedUnMixMC modeling indicated that the fine-grained feldspar, quartz- and Zr-rich layer in core 02PC (IRD2B) dated at ~13 ka cal BP is mainly derived from the Mackenzie River (40%, Figure 6h). Optically stimulated luminescence ages from the Mackenzie drainage basin suggest a major routing of deglacial meltwaters from Lake Agassiz into the Arctic Ocean at 13 ± 0.2 ka cal BP, near the onset of the Younger Dryas (Murton et al., 2010). This observation concurred to highlight that the quartz- and feldspars-rich layers observed at ~13 ka cal BP in the Canadian Beaufort margin may be related to an outburst flood from Lake Agassiz. We hypothesize that meltwaters from the Lake Agassiz remobilized rock flour deposits that are characterized by an abundance of quartz and feldspars from the northwest part of the Mackenzie River watershed (Figure 8). Furthermore, SedUnMixMC modeling also indicated that dolomite-rich (Ca-Mg) IRD layers (IRD1A and IRD2A) dated at 11 and 12.8 ka cal BP originated from the Canadian Arctic Archipelago (Figure 6h). Similar dolomite-rich IRDs have been found on the Lomonosov Ridge and in Fram Strait during the Younger Dryas chronozone (Hillaire-Marcel et al., 2013; Maccali et al., 2013; Not & Hillaire-Marcel, 2012). Major purge from the M'Clure and Amundsen Gulf ice stream was previously suggested by isotope data (Hillaire-Marcel et al., 2013; Maccali et al., 2013), paleogeography study (Stokes et al., 2009), and numerical model (Tarasov & Peltier, 2005) between 13 and 12.7 ka cal BP and may have played a role in the slowdown of the Atlantic Meridional Overturning Circulation at the onset of the Younger Drays (Condron & Winsor, 2012). Overall, our results support the hypothesis that large meltwater and iceberg discharges from the Lake Agassiz outburst and Amundsen Gulf ice stream were likely to have triggered the Younger Dryas cooling by inhibiting deep water formation in the subpolar North Atlantic and weakening the strength of the Atlantic Meridional Overturning Circulation (Condron & Winsor, 2012; Hillaire-Marcel et al., 2013; Lakeman et al., 2018; Maccali et al., 2013; Not & Hillaire-Marcel, 2012; Tarasov & Peltier, 2005).

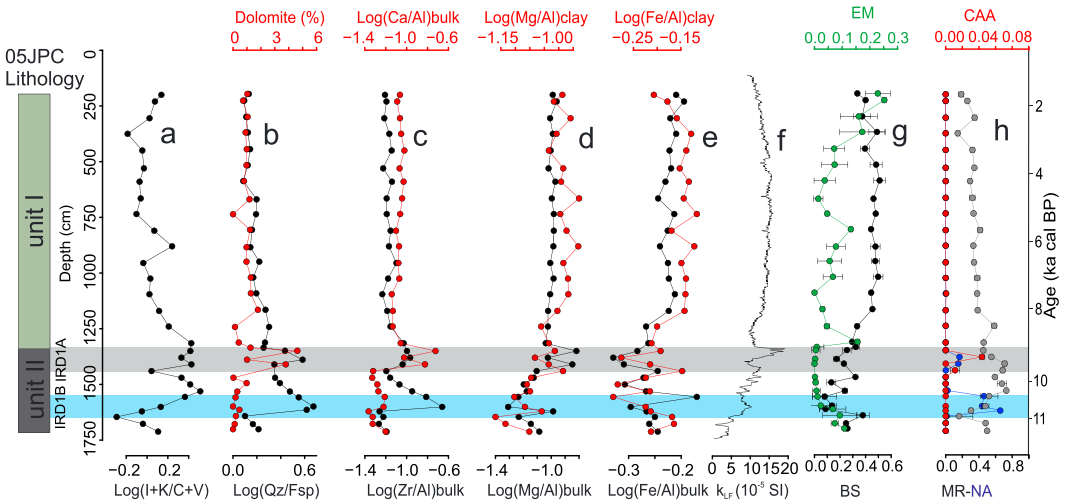

Figure 7. Downcore variations of core 05JPC showing (a) log-ratio illite + kaolinite/chlorite. (b) Log-ratio quartz/feldspar (black) and proportion of dolomite (red). (c) Log-ratio Zr/Al (black) and Ca/Al (red). (d) Log-ratio Mg/Al for the bulk (black) and clay (red) fractions. (e) Log-ratio Fe/Al for the bulk (black) and clay (red) fractions. (f) Magnetic susceptibility, k_{lf} (Barletta et al., 2008). (g) Proportion of sediment from the Eurasian margin (EM), which includes Kara Sea and Eastern Siberian Sea in green and proportion of sediment from the Bering Strait in black. (h) Proportion of sediment from the Mackenzie River (black), North Alaska (blue), and CAA (red). IRD layers rich in dolomite and quartz are highlighted in gray and blue, respectively. IRD = ice-rafted debris.

In core 02PC, the high quartz/total feldspars and phyllosilicates/total feldspars ratios observed during the Younger Dryas interval suggest that the detrital sediments mainly originated from the northern tributaries of the Mackenzie River (Figures 6 and 8a). Wickert (2016) suggested that meltwater inputs to the Mackenzie River ended no later than 11 ka cal BP, when its eastern tributaries were temporarily rerouted eastward due to a combination of ice retreat and glacial isostatic depression. The age of 11 ka cal BP coincides with the decrease of the sedimentation rates from 50 to 2 cm/ka (Figure S1). In addition, the low foraminifera abundance and high terrestrial organic matter content observed in the nearby core 750PC (Scott et al., 2009) also suggest higher Mackenzie River discharge to the Canadian Beaufort margin during this time, providing support to our interpretations. Finally, in agreement with Stokes et al. (2005, 2009, 2006) and Dyke and Savelle (2000), we suggest that the IRD1A layers dated at 11 ka cal BP may be linked to a retreat phase of the Amundsen Gulf Ice Stream occurring during the meltwater pulse 1B (Figure 8b).

5.1.2. Chukchi-Alaskan Margin

The overall mineralogical and geochemical signatures characterizing core 05JPC around 11 ka cal BP point to a detrital input from the Bering Strait and Eurasian margin (~30% each; Figure 6g). However, the increase of vermiculite and mixed-layer chlorite/smectite recorded in the clay fraction in this interval together with lower Log (EM1/EM2) ratio suggests that most of the sediments are mainly derived from the Bering Strait and redistributed by bottom (nepheloid) currents to the shelf and continental slope (Figures 9 and S3). In addition, amorphous silica concentrations, derived from qXRD analysis, also depict a sharp increase (up to 25%) in the same interval (Figure 9). High amorphous silica concentrations in the Chukchi Sea sediments are interpreted to represent times when biosilica-rich Pacific waters flowed through the Bering Strait (Jakobsson et al., 2017). Indeed, the presence of amorphous silica, including diatoms, radiolarians, siliceous sponges, and silicoflagellates, is a characteristic signature of Pacific waters today, and therefore, this proxy may also be used to track Pacific waters inflow in the western Arctic Ocean (Jakobsson et al., 2017; Stein et al., 2017). Thus, we hypothesize that sediments in this interval may be related to the initial opening of the Bering Strait at ~11 ka cal BP (Jakobsson et al., 2017).

SedUnMixMC results from core 05JPC suggest that the fine-grained quartz and Zr-rich IRD layers and dolomite-rich (Ca-Mg) IRD layers originate from the Northwest Alaska and the Canadian Arctic Archipelago, respectively (Figure 7h). The quartz- and Zr-rich, but carbonate-poor, sediment record at ~10.6 ka cal BP (IRD1B) is more consistent with a northwestern Alaskan source (Polyak et al., 2007). Indeed, high-resolution seismic reflection data in conjunction with sedimentological data from piston cores from the outer

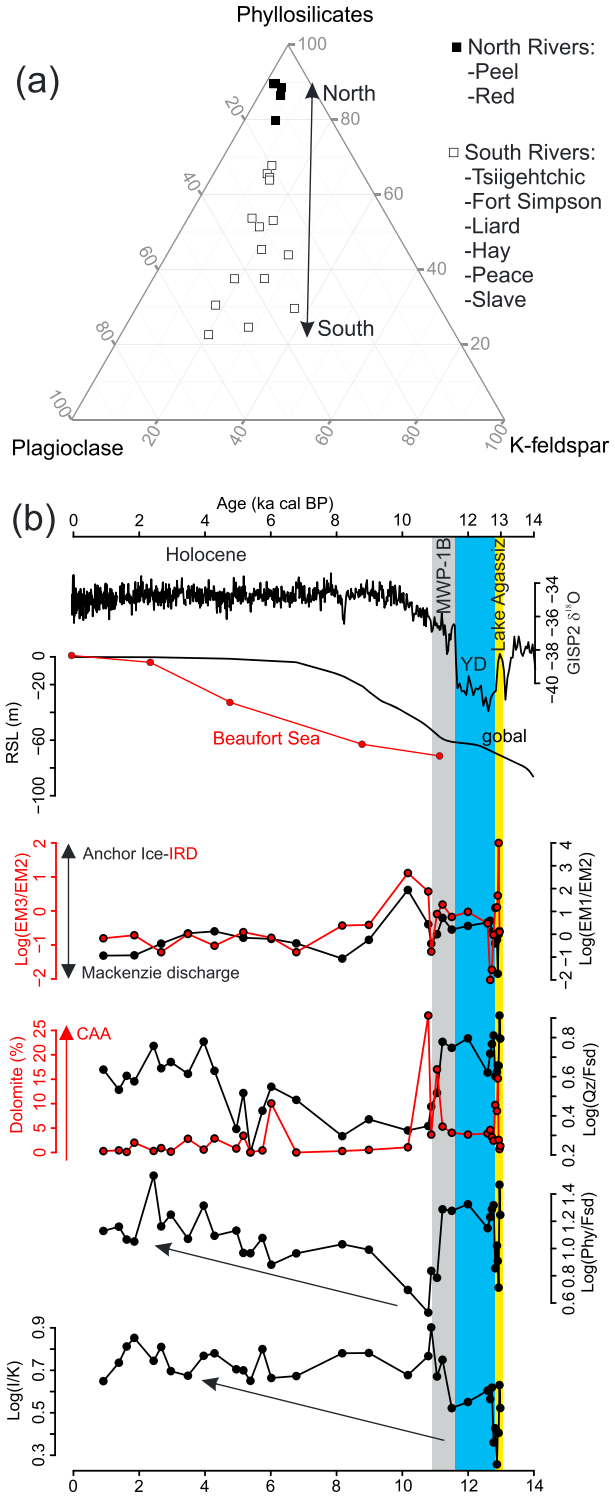

Figure 8. (a) Phyllosilicates-plagioclase-K-feldspar ternary plot of sand samples from the main tributaries of the Mackenzie River (Gamboa, 2017). Note that the northern tributaries are enriched in phyllosilicates, while the southern tributaries are enriched in total feldspars. (b) Comparison of Log (EM3/EM2), Log (EM1/EM2), Log (Qz/Fsd), dolomite content, Log (Phy/Fsd) and Log (I/K) from core 02PC with global eustatic sea level variations (Lambeck et al., 2014) and relative sea level from the Beaufort Sea (Héquette et al., 1995). IRD = ice-rafted debris; BP = before present.

Chukchi margin are evidence of the occurrence of meltwater discharges from the Brooks Range to the shelf occurring between 10 and 13 ka cal BP (Hill & Driscoll, 2008, 2010). At the opposite, the carbonate-rich layers dated at 9.5 ka cal BP are more consistent with the Canadian Archipelago source. We infer that the dolomite-rich IRD (IRD1A) layer at 9.5 ka cal BP may be related to the final retreat phase of the Amundsen Gulf Ice Stream which ceased operating by ~9.5 ka cal BP (Stokes et al., 2009). However, this carbonate-rich layer is missing in the Canadian Beaufort margin, as such layer was not identified in core 02PC at this time (Figure 6). A plausible explanation for this could be the presence of a hiatus in the early to middle Holocene transition (Figure S1b). This observation is supported by the fact that sedimentation rates in core 02PC show a distinct decrease from 50 to 2 cm/ka between 6 and 11 ka cal BP, which appears very large and abrupt. However, the accumulation is thought to have been continuous because of the lack of sharp lithological changes or sedimentological indicators of hiatus or mass flow transport in this part of the core (Deschamps et al., 2017). In addition, this abrupt decrease in sedimentation rates is consistent with major reduction of meltwater flow derived from the Mackenzie River (Wickert, 2016). Alternatively, as ages after 8.5–9 ka cal BP in core 05JPC were extrapolated, and the IRD1A in cores 05JPC and 02PC show similar mineralogical and geochemical signatures, which are consistent with a common source area (Figure 4). We thus hypothesize that the dolomite-rich IRD1A in core 05JPC could be dated at 11 ka cal BP similar to IRD1A from core 02PC (Figure S1a). This IRD correlation would imply that the age for the opening of the Bering Strait may be older than 11 ka cal BP (Jakobsson et al., 2017) as previously suggested by Keigwin et al. (2006), England and Furze (2008), and Elias et al. (1992). Further investigations are required to gain a more precise chronology of the age constraint for the Bering Land Bridge flooding.

5.2. Holocene Sediment Dynamics (10.5 ka cal BP to Present)

5.2.1. Canadian Beaufort Sea

In the Canadian Beaufort margin, the Log (EM1/EM2) ratio from the core 02PC showed few variations from 10 ka cal BP to present, supporting the idea that stable sedimentation dynamic dominate throughout the Holocene (Figure 8b). Likewise, the sediment unmixing model suggests that Holocene detrital sediments are derived primarily from the Mackenzie River (>80%; Figures 7h and 10). However, the slight changes observed in bulk and clay mineralogical signatures during the middle Holocene relative to the deglacial interval (i.e., relatively enriched in total feldspars and illite; Figure 8b) may reflect changes in sediment provenance within the Mackenzie River basin. Indeed, the watershed lithology of the main Mackenzie River tributaries is composed of a mixture between shale and igneous rocks having granodioritic to granitic compositions (Dellinger et al., 2017; Millot et al., 2003). More specifically, the northern tributaries of the Mackenzie River (such as the Peel and Red Rivers) drain almost exclusively weathered marine sedimentary rocks (e.g., Cambrian to Cretaceous limestones and shales), which are enriched in phyllosilicates, quartz, and detrital carbonates, whereas granitic source rocks outcropping in the North American Cordillera (including the Rocky and the Mackenzie Mountains) and Canadian Shield are drained by the southern tributaries (such as the Liard and Slave Rivers), which are characterized by an abundance of total feldspars (Gamboa, 2017; Figure 8a). All these observations suggest that the proportion of sediments derived from the southern

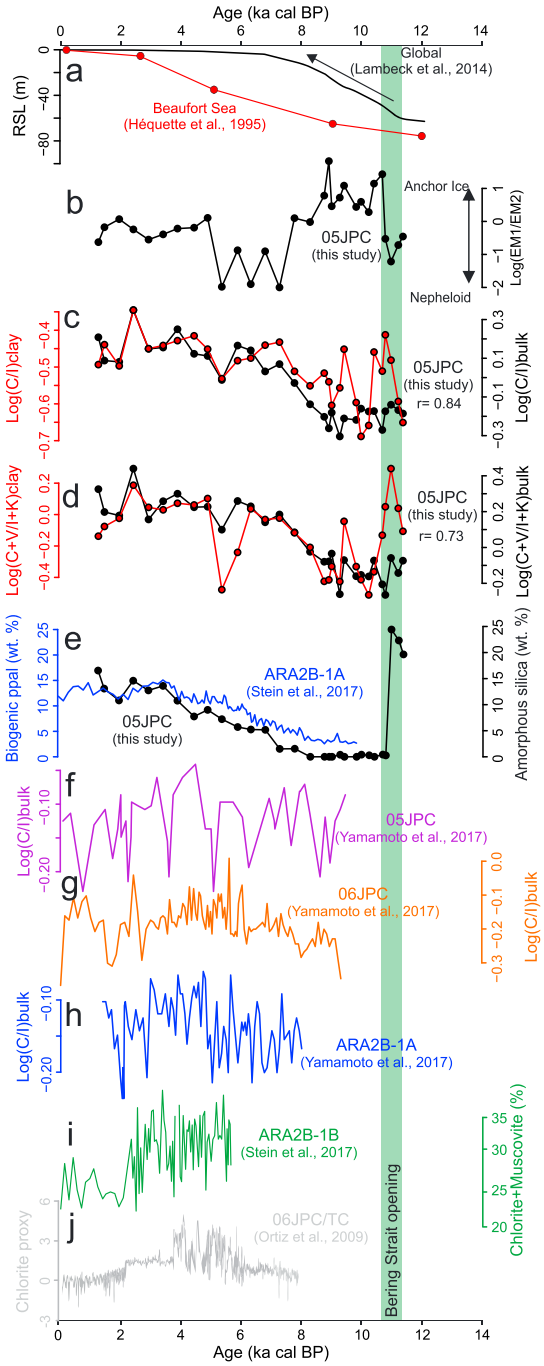

Figure 9. Comparison of (a) global eustatic sea level changes and relative sea level variation in the Beaufort Sea, (b) Log (EM1/EM2) for cores 05JPC, (c) log-ratio chlorite/illite based on bulk (black) and clay mineralogy (red) from core 05JPC, (d) Log-ratio chlorite + vermiculite/illite + kaolinite based on bulk (black) and clay mineralogy (red) from core 05JPC, (e) amorphous silica from core 05JPC (black) and biogenic opal for the core ARA2B-1A (blue), (f) Log-ratio chlorite/illite derived of the bulk mineralogy from core 05JPC, (g) Log-ratio chlorite/illite of the bulk mineralogy from core 06JPC, (h) Log-ratio chlorite/illite of the bulk mineralogy from core ARA2B-1A, (i) Chlorite+ muscovite contents from core ARA2B-1B, and (j) chlorite proxy obtained by diffusive spectral reflectance analysis from cores 06JPC/TC. Opening of the Bering Strait is highlighted in light green.

tributaries increased during the middle Holocene. Thus, we hypothesized that the final recession of the Laurentide Ice Sheet in the Mackenzie Valley after ~11–10.5 ka cal BP (Dyke, 2004) promoted a major remobilization of glaciogenic sediments derived from crystalline rocks as the Mackenzie River adjusted to the postglacial hydrologic regime. Alternatively, we cannot rule out the possibility that Holocene changes in relative sea level could also influence sedimentation in the Canadian Beaufort margin (Figure 8b). The sea level rise resulted in coastal retreat and likely exerted significant control on the sedimentation on the Mackenzie Shelf during the early to middle Holocene (Héquette et al., 1995). A minor proportion of fine silt detrital sediments in core 02PC during the middle Holocene may therefore also been supplied from sea level rise-induced coastal erosion of fine-grained Pleistocene quartz- and feldspar-rich glacial tills outcropping along the Tuktoyaktuk Peninsula (Gamboa et al., 2017; Vogt, 1997; Figure 8b). However, sediments from the southern Mackenzie River tributaries and Tuktoyaktuk Peninsula are both characterized by similar mineralogical signatures (Gamboa, 2017), and therefore, we cannot estimate the proportion of sediment derived from coastal erosion. Additional information could be gained by consideration of other provenance indicators such as radiogenic isotopes (Fagel et al., 2014).

5.2.2. Chukchi-Alaskan Margin

SedUnMixMC modeling and the mineralogical ratios Log (I + K/C + V) and Log (Qz/Fsp) from core 05JPC indicate that during the early Holocene (10.5–8 ka cal BP), the predominant sediment source on the Chukchi-Alaskan margin was from the Mackenzie River (up to 92%). In addition, Log (EM1/EM2) ratios revealed the dominance of clay- to fine silt-size particles during the early Holocene, suggesting that sediment transport by sea ice predominates at this time (Figures 7h and 9b). In accordance with previous sedimentological studies (Darby et al., 2012; Not & Hillaire-Marcel, 2012; Yamamoto et al., 2017), we hypothesize that sediment-laden meltwater plumes derived from glacial erosion on the Mackenzie River basin were incorporated on the shelf by sea ice. Sea ice was thus transported westward along the Chukchi-Alaskan margin by an enhanced BG during the early Holocene (Figure 10). Note that the BG strengthening during the early Holocene is likely driven by a maximum boreal summer insolation (Gajewski, 2015; Yamamoto et al., 2017).

During the Holocene, the Log (EM1/EM2) ratio reached minimum values between 8 and 6 ka cal BP, suggesting that sediment transport during the middle Holocene was dominated by bottom currents (Figure 9b). In addition, the end-member EM3 (10 to 30 μm) records from both margins during the deglacial interval are clearly associated with the IRD events (Figure 3b). However, this EM is still present during the Holocene interval for cores located in the Chukchi-Alaskan margin (01JPC and 05JPC), while it did not influence the Holocene sedimentation in the Canadian Beaufort shelf (Figure 3b). In agreement with previous late Quaternary sedimentological and geochemical studies from the western Arctic (Darby et al., 2009), we hypothesize that end-member EM3 recorded in the Holocene sediments from the Chukchi-Alaskan margin may reflect suspended load and winnowed silts deposited by downwelling of brine-enriched shelf waters. Moreover, the SedUnMixMC modeling reveals that sediment provenance in core 05JPC was mainly derived from the Bering Strait, Mackenzie River, and Eurasian margin (Figures 7g and 7h). The

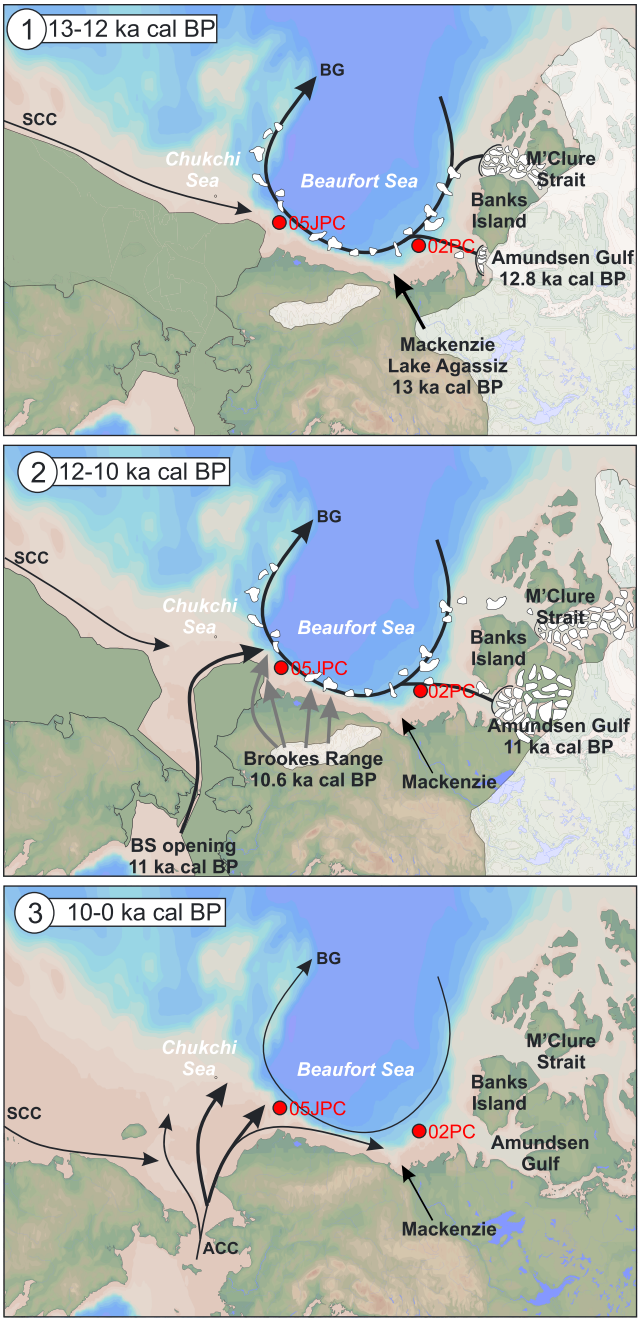

Figure 10. Evolution of sedimentary dynamics in the western Arctic Ocean during the last 13 ka cal before present (BP).

proportion of sediment derived from the Mackenzie River gradually decreases upcore (60 to 30%), whereas the Bering Strait and Eurasian margin sources show a long-term increase (10 to 60% and 0 to 30%; Figures 7i and 7j). Indeed, decreases of quartz, kaolinite, illite, aluminum, and potassium contents most likely reflect a decline in sediment inputs from the Mackenzie River (Figure 7), while an increase of total feldspars, chlorite, muscovite, and vermiculite, as well as magnesium and iron contents in the clay fraction reflect higher Bering Strait sediment inputs (Figures 7d, 7e, and S3). Thus, the Holocene variations observed in the detrital proxies from core 05JPC are likely related to a long-term decline in both the Mackenzie River discharge (Wagner et al., 2011) and anchor ice transported by weaker BG (Yamamoto et al., 2017). In addition, the increased proportion of sediment coming from the Kara Sea observed in core 05JPC between 4 and 2 ka cal BP (15–30%; Figure 7g) suggests that a strong positive mode of the AO was predominant at this time (Darby et al., 2012). In fact, based on iron oxide grain provenance on the Chukchi shelf and slope sediments, Darby and Bischof (2004) and Darby et al. (2012) suggested a weaker BG during the late Holocene, which also occurs today during the positive phase of the AO in agreement with our interpretations (Figure 10).

As shown in Figures 7a, 7b, 7g, 9c, and 9d, the proportion of chlorite, vermiculite, total feldspars, amorphous silica, and sediments derived from the Bering Strait showed a gradual increase between 10 and 2 ka cal BP, with maximum values recorded between 7.5 and 2 ka cal BP, suggesting an enhanced increase in the Bearing Strait inflow into the Chukchi Sea. This increased Bearing Strait inflow trend shows a parallel temporal evolution with regional sea level variations and increasing bottom current redistribution (Figures 3–9). In agreement with Keigwin et al. (2006), we hypothesize that the progressive and rapid relative sea level rise observed during 10 and 7.5 ka cal BP in the western Arctic Ocean promoted not only the widening and deepening of the Bering Strait but also the subsequent remobilization of sediments stored on the Chukchi Shelf and the enhanced sediment transport from the Pacific toward the western Arctic Ocean (Figure 10). Our findings are consistent with palynological (dinocyt, pollen, and spores) and organic matter geochemistry data from the same sediment core (Faux et al., 2011; Khim et al., 2018; McKay et al., 2008; Polyak et al., 2016), indicating that full marine continental shelf setting was established in the Chukchi-Alaskan margin between 7 and 8 ka cal BP. Overall, these observations suggest that regional sea level variations have exerted a significant control on sedimentation in the western Arctic Ocean during the early to middle Holocene.

As a whole, although the variations in the previously published mineralogical proxy records of the Bearing Strait inflow are not identical among the different sediment cores from the Chukchi Sea (Figures 9e–9i; Ortiz et al., 2009; Stein et al., 2017; Yamamoto et al., 2017), there is a common enhancement in the Bering Strait inflow between 7.5 and 2 ka cal BP, followed by a decrease during the last 2 ka cal BP (Ortiz et al., 2009; Stein et al., 2017; Yamamoto et al., 2017). Holocene changes in the Bering Strait inflow have been attributed to changes in the Aleutian Low pressure system, which is located in the North Pacific (Yamamoto et al., 2017). This Aleutian Low is sensitive to tropical Pacific sea surface temperature (SST) anomalies (Anderson et al., 2016; Osterberg et al., 2014; Trenberth & Hurrell, 1994). In general, warm eastern Pacific SST conditions are characterized by a stronger and southeastward shifted Aleutian Low, while cool eastern Pacific SSTs conditions are associated with a weaker and northwestward shifted Aleutian Low. In this context, the Holocene paleoenvironmental records across eastern Beringia (Alaska, westernmost Canada, and adjacent seas) suggest that the

Aleutian Low was weaker during the middle Holocene than during the late Holocene (Barron & Anderson, 2011). This configuration is thought to promote a major Bering Strait inflow into the Chukchi Sea during the middle Holocene and a weak inflow during the late Holocene. Finally, as discussed in Darby and Bischof (2004) and Yamamoto et al. (2017), sediments transported by the inflowing Pacific waters into the Bering Strait might be diverted west toward Herald Canyon by the western Bering Sea branches, and thus missing the Chukchi-Alaskan margin (Yamamoto et al., 2017). This redistribution of the Bering Strait inflow between the different current branches may be a plausible explanation for the spatial and temporal differences observed between the Pacific inflow proxies from the Chukchi Sea cores (Figure 9).

6. Summary and Conclusions

Geochemical and mineralogical compositions of two sediment cores recovered on the Canadian Beaufort (core 02PC) and Chukchi-Alaskan (core 05JPC) margins highlight the evolution of the origin, transport, and dynamics of the detrital sediments in the western Arctic Ocean since deglaciation. Overall, the results of this research yield the following generalizations and conclusions:

1. The EM modeling analysis of grain-size data indicates that sea ice and nepheloid current are factors controlling sediment redistribution in the Chukchi-Alaskan margin, whereas sea ice and the Mackenzie River sediment plume influenced sedimentation in the Canadian Beaufort margin.
2. The mineralogical and geochemical data from the bulk and clay fractions corroborate that Log (I + K/C + V), Log (Qz/Fsp), dolomite, Log (Ca/Al), Log (Mg/Al), and Log (Fe/Al), together with a discriminant diagram based on Al − Si − Ca and I + K − total feldspars − dolomite, can be successfully used to track changes in detrital sediment provenance on the Chukchi and Beaufort continental margins.
3. The sediment unmixing model, together with specific mineralogical and geochemical signatures, indicates that the North American margin (including the Mackenzie River, Northern Alaska, and Canadian Arctic Archipelago) is the major source of sediment during the deglaciation at the coring sites of cores 05JPC and 02PC.
4. The dolomite-rich IRD layers dated to 12.8 and 11 ka cal BP in core 02PC and 9.5 ka cal BP in core 05JPC are related to the debacle of the M'Clure and Amundsen Ice Streams. The quartz and feldspar-rich IRD intervals dated to 13 ka cal BP in core 02PC and 10.7 ka cal BP in core 05JPC are likely related to meltwater events and are derived from the Mackenzie River and the Brooks Range glaciers in the northwestern Alaska, respectively.
5. Mineralogical and geochemical signatures of deglacial sediments from core 02PC support the hypothesis that large meltwater and iceberg discharges from the Lake Agassiz outburst through the Mackenzie Valley may have triggered the Younger Dryas cooling.
6. During the Holocene, the detrital sediment supply in the Canadian Beaufort margin remains controlled mainly by the Mackenzie River. In the Chukchi margin, the proportion of sediment derived from the Mackenzie River gradually decreased during the early to late Holocene.
7. The opening of the Bering Strait at 11 ka cal BP is typified in core 05JPC by a sharp increase in vermiculite, mixed-layer chlorite/smectite, and amorphous silica. In addition, bulk mineralogical data, together with high Log (Mg/Al) and Log (Fe/Al) ratios from the clay fraction, support the notion that an enhanced Bearing Strait inflow into the Chukchi Sea occurred between 7.5 and 2 ka cal BP.
8. The similar trends observed between the regional sea level curves and our mineralogical and geochemical data suggest that the relative sea level changes in the western Arctic Ocean have an important influence on the western Arctic sedimentary dynamics during the early to middle Holocene.

Acknowledgments
We sincerely thank the captains, officers, crew, and scientists on board the USCGC Healy and the CCGS Amundsen for the recovery the cores used in this study. These cores were collected as part of the HOTRAX expedition (USCGC Healy), as well as the CASES and ArcticNet (CCGS Amundsen) programs. We also thank Quentin Beauvais (UQAR-ISMER), Mathieu Babin (UQAR-ISMER), and Adriana Gamboa (UQAR-ISMER and UDO) for their technical support and advice in the laboratory. This research was funded by ArcticNet and by the Natural Sciences and Engineering Research Council of Canada (NSERC) through discovery grants to J.-C Montero-Serrano and G. St-Onge, as well as through ship time support for several expeditions (J.-C. Montero-Serrano and G. St-Onge). J.-C. Montero-Serrabo thanks Dr. Mathieu Dellinger of the Durham University for kindly providing bed sands samples from the Mackenzie River basin. Lastly, thanks to the reviewer John T. Andrews for improving this article through careful review and to Yusuke Yokoyama for his editorial work. All analytical data presented are available electronically in the PANGAEA database (https://www.pangaea.de/).

References

Aitchison, J. (1990). Relative variation diagrams for describing patterns of compositional variability. *Mathematical Geology*, *22*(4), 487–511. https://doi.org/10.1007/BF00890330

Anderson, L., Berkelhammer, M., Barron, J. A., Steinman, B. A., Finney, B. P., & Abbott, M. B. (2016). Lake oxygen isotopes as recorders of North American Rocky Mountain hydroclimate: Holocene patterns and variability at multi-decadal to millennial time scales. *Global and Planetary Change*, *137*, 131–148. https://doi.org/10.1016/j.gloplacha.2015.12.021

Andrews, J. T. (2000). Icebergs and iceberg rafted detritus (IRD) in the North Atlantic: Facts and assumptions. *Oceanography*, *13*, 100–108.

Andrews, J. T., Bjork, A. A., Eberl, D. D., Jennings, A. E., & Verplanck, E. P. (2015). Significant differences in late Quaternary bedrock erosion and transport: East versus West Greenland ~70°N—Evidence from the mineralogy of offshore glacial marine sediments. *Journal of Quaternary Science*, *30*(5), 452–463. https://doi.org/10.1002/jqs.2787

Andrews, J. T., & Eberl, D. D. (2012). Determination of sediment provenance by unmixing the mineralogy of source-area sediments: The "SedUnMix" program. *Marine Geology*, *291-294*, 24–33. https://doi.org/10.1016/j.margeo.2011.10.007

Andrews, J. T., Stein, R., Moros, M., & Perner, K. (2016). Late Quaternary changes in sediment composition on the NE Greenland margin (~73°N) with a focus on the fjords and shelf. *Boreas*, *45*(3), 381–397. https://doi.org/10.1111/bor.12169

Andrews, J. T., & Vogt, C. (2014). Source to sink: Statistical identification of regional variations in the mineralogy of surface sediments in the western Nordic Seas (58°N–75°N; 10°W–40°W). *Marine Geology*, *357*, 151–162. https://doi.org/10.1016/j.margeo.2014.08.005

Asahara, Y., Takeuchi, F., Nagashima, K., Harada, N., Yamamoto, K., Oguri, K., & Tadai, O. (2012). Provenance of terrigenous detritus of the surface sediments in the Bering and Chukchi Seas as derived from Sr and Nd isotopes: Implications for recent climate change in the Arctic regions. *Deep-Sea Research Part II: Topical Studies in Oceanography*, *61-64*, 155–171. https://doi.org/10.1016/j.dsr2.2011.12.004

Astakhov, A. S., Rujian, W., Crane, K., Ivanov, M. V., & Aiguo, G. (2013). Lithochemical classification of the arctic depositional environments (Chukchi Sea) by methods of multivariate statistic. *Geochemistry International*, *51*, 269–289. https://doi.org/10.1134/S001670291302002X

Barletta, F., St-Onge, G., Channell, J. E. T., Rochon, A., Polyak, L., & Darby, D. (2008). High-resolution paleomagnetic secular variation and relative paleointensity records from the western Canadian Arctic: Implication for Holocene stratigraphy and geomagnetic field behaviour. *Canadian Journal of Earth Sciences*, *45*(11), 1265–1281. https://doi.org/10.1139/E08-039

Barron, J. A., & Anderson, L. (2011). Enhanced Late Holocene ENSO/PDO expression along the margins of the eastern North Pacific. *Quaternary International*, *235*(1-2), 3–12. https://doi.org/10.1016/j.quaint.2010.02.026

Belt, S. T., Vare, L. L., Massé, G., Manners, H. R., Price, J. C., MacLachlan, S. E., et al. (2010). Striking similarities in temporal changes to spring sea ice occurrence across the central Canadian Arctic Archipelago over the last 7000 years. *Quaternary Science Reviews*, *29*(25-26), 3489–3504. https://doi.org/10.1016/j.quascirev.2010.06.041

Biscaye, P. E. (1965). Mineralogy and sedimentation of recent deep-sea clay in the Atlantic Ocean and adjacent seas and oceans. *Geological Society of America Bulletin*, *76*(7), 803–832. https://doi.org/10.1130/0016-7606(1965)76

Bischof, J. F., & Darby, D. A. (1999). Quaternary ice transport in the Canadian Arctic and extent of Late Wisconsinan Glaciation in the Queen Elizabeth Islands. *Canadian Journal of Earth Sciences*, *36*(12), 2007–2022. https://doi.org/10.1139/e99-096

Blaauw, M., & Christen, A. (2011). Flexible paleoclimate age-depth models using an autoregressive gamma process. *Bayesian Analysis*, *6*(3), 457–474. https://doi.org/10.1214/11-BA618

Blott, S. J., & Pye, K. (2001). GRADISTAT: A grain size distribution and statistic package for the analysis of unconsolidated sediments. *Earth Surface Processes and Landforms*, *26*(11), 1237–1248. https://doi.org/10.1002/esp.261

Bout-Roumazeilles, V., Cortijo, E., Labeyrie, L., & Debrabant, P. (1999). Clay mineral evidence of nepheloid layer contributions to the Heinrich layers in the northwest Atlantic. *Palaeogeography, Palaeoclimatology, Palaeoecology*, *146*(1-4), 211–228. https://doi.org/10.1016/S0031-0182(98)00137-0

Condron, A., & Winsor, P. (2012). Meltwater routing and the Younger Dryas. *Proceedings of the National Academy of Sciences of the United States of America*, *109*, 19,928–19,933. https://doi.org/10.1073/pnas.1207381109

Coulthard, R. D., Furze, M. F. A., Pieńkowski, A. J., Chantel Nixon, F., & England, J. H. (2010). New marine ΔR values for Arctic Canada. *Quaternary Geochronology*, *5*(4), 419–434. https://doi.org/10.1016/j.quageo.2010.03.002

Danielson, S. L., Weingartner, T. J., Hedstrom, K. S., Aagaard, K., Woodgate, R., Curchitser, E., & Stabeno, P. J. (2014). Coupled wind-forced controls of the Bering–Chukchi shelf circulation and the Bering Strait throughflow: Ekman transport, continental shelf waves, and variations of the Pacific–Arctic sea surface height gradient. *Progress in Oceanography*, *125*, 40–61. https://doi.org/10.1016/j.pocean.2014.04.006

Darby, D. A., & Bischof, J. F. (2004). A Holocene record of changing Arctic Ocean ice drift analogous to the effects of the Arctic Oscillation. *Paleoceanography*, *19*, PA1027. https://doi.org/10.1029/2003PA000961

Darby, D. A., Jakobsson, M., & Polyak, L. (2005). Icebreaker expedition collects key Arctic seafloor and ice data. *Eos, Transactions American Geophysical Union*, *86*(52), 549–549. https://doi.org/10.1029/2005EO520001

Darby, D. A., Myers, W. B., Jakobsson, M., & Rigor, I. (2011). Modern dirty sea ice characteristics and sources: The role of anchor ice. *Journal of Geophysical Research: Oceans*, *116*, C09008. https://doi.org/10.1029/2010JC006675

Darby, D. A., Ortiz, J., Polyak, L., Lund, S., Jakobsson, M., & Woodgate, R. A. (2009). The role of currents and sea ice in both slowly deposited central Arctic and rapidly deposited Chukchi-Alaskan margin sediments. *Global and Planetary Change*, *68*(1-2), 58–72. https://doi.org/10.1016/j.gloplacha.2009.02.007

Darby, D. A., Ortiz, J. D., Grosch, C. E., & Lund, S. P. (2012). 1,500-year cycle in the Arctic Oscillation identified in Holocene Arctic sea-ice drift. *Nature Geoscience*, *5*(12), 897–900. https://doi.org/10.1038/ngeo1629

Darby, D. A., & Zimmerman, P. (2008). Ice-rafted detritus events in the Arctic during the last glacial interval, and the timing of the Innuitian and Laurentide ice sheet calving events. *Polar Research*, *27*, 114–127. https://doi.org/10.1111/j.1751-8369.2008.00057.x

Dellinger, M., Bouchez, J., Gaillardet, J., Faure, L., & Moureau, J. (2017). Tracing weathering regimes using the lithium isotope composition of detrital sediments. *Geology*, *45*(5), 411–414. https://doi.org/10.1130/G38671.1

Deschamps, C.-E., St-Onge, G., Montero-Serrano, J.-C., & Polyak, L. (2017). Chronostratigraphy and spatial distribution of the Chukchi and Beaufort seas since the last deglaciation. *Boreas*, *47*(2), 544–564. https://doi.org/10.1111/bor.12296

Dietze, E., Hartmann, K., Diekmann, B., Ijmker, J., Lehmkuhl, F., Opitz, S., et al. (2012). An end-member algorithm for deciphering modern detrital processes from lake sediments of Lake Donggi Cona, NE Tibetan Plateau, China. *Sedimentary Geology*, *243-244*, 169–180. https://doi.org/10.1016/j.sedgeo.2011.09.014

Dong, L., Liu, Y., Shi, X., Polyak, L., Huang, Y., Fang, X., et al. (2017). Sedimentary record from the Canada Basin, Arctic Ocean: Implications for late to middle Pleistocene glacial history. *Climate of the Past*, *13*, 1–60. https://doi.org/10.5194/cp-2016-139

Dyke, A. S. (2004). An outline of the deglaciation of North America with emphasis on central and northern Canada. *Quaternary Glaciations-Extent and Chronology, Part II: North America*, *2b*, 373–424. https://doi.org/10.1016/S1571-0866(04)80209-4

Dyke, A. S., & Savelle, J. M. (2000). Major end moraines of Younger Dryas age on Wollaston Peninsula, Victoria Island, Canadian Arctic: Implications for paleoclimate and for formation of hummocky moraine. *Canadian Journal of Earth Sciences*, *38*(6), 1003–1006. https://doi.org/10.1139/cjes-38-6-1003

Eberl, D. D. (2003). User guide to RockJock—A program for determining quantitative mineralogy from X-ray diffraction data. USGS Open File Report, OF 03-78, 40.

Eberl, D. D. (2004). Quantitative mineralogy of the Yukon River system: Changes with reach and season, and determining sediment provenance. *American Mineralogist*, *89*(11-12), 1784–1794. https://doi.org/10.2138/am-2004-11-1225

El Ouahabi, M., Hubert-Ferrari, A., & Fagel, N. (2017). Lacustrine clay mineral assemblages as a proxy for land-use and climate changes over the last 4 kyr: The Amik Lake case study, Southern Turkey. *Quaternary International*, *438*, 15–29. https://doi.org/10.1016/j.quaint.2016.11.032

Elias, S. A., Short, S. K., & Phillips, R. L. (1992). Paleoecology of late-glacial peats from the Bering Land Bridge, Chukchi Sea Shelf Region, Northwestern Alaska. *Quaternary Research*, *38*(3), 371–378. https://doi.org/10.1016/0033-5894(92)90045-K

England, J. H., & Furze, M. F. A. (2008). New evidence from the western Canadian Arctic Archipelago for the resubmergence of Bering Strait. *Quaternary Research*, *70*(1), 60–67. https://doi.org/10.1016/j.yqres.2008.03.001

Fagel, N., Not, C., Gueibe, J., Mattielli, N., & Bazhenova, E. (2014). Late Quaternary evolution of sediment provenances in the Central Arctic Ocean: Mineral assemblage, trace element composition and Nd and Pb isotope fingerprints of detrital fraction from the Northern Mendeleev Ridge. *Quaternary Science Reviews*, *92*, 140–154. https://doi.org/10.1016/j.quascirev.2013.12.011

Faux, J. F., Belicka, L. L., & Rodger Harvey, H. (2011). Organic sources and carbon sequestration in Holocene shelf sediments from the western Arctic Ocean. *Continental Shelf Research*, *31*(11), 1169–1179. https://doi.org/10.1016/j.csr.2011.04.001

Forest, A., Tremblay, J. é., Gratton, Y., Martin, J., Gagnon, J., Darnis, G., et al. (2011). Biogenic carbon flows through the planktonic food web of the Amundsen Gulf (Arctic Ocean): A synthesis of field measurements and inverse modeling analyses. *Progress in Oceanography*, *91*(4), 410–436. https://doi.org/10.1016/j.pocean.2011.05.002

Gajewski, K. (2015). Quantitative reconstruction of Holocene temperatures across the Canadian Arctic and Greenland. *Global and Planetary Change*, *128*, 14–23. https://doi.org/10.1016/j.gloplacha.2015.02.003

Gamboa, A. 2017: Evaluación de la dinámica sedimentaria del margen continental del mar de Beaufort y golfo de Amundsen (Océano Ártico): Implicaciones paleoceanográficas y paleoclimáticas durante el Holoceno. Universidad de Oriente. 240 pp.

Gamboa, A., Montero-Serrano, J.-C., St-Onge, G., Rochon, A., & Desiage, P.-A. (2017). Mineralogical, geochemical and magnetic signatures of surface sediments from the Canadian Beaufort Shelf and Amundsen Gulf (Canadian Arctic). *Geochemistry, Geophysics, Geosystems*, *18*, 488–512. https://doi.org/10.1002/2016GC006477

Gardner, J. V., Dean, W. E., & Vallier, T. L. (1980). Sedimentology and geochemistry of surface sediments, outer continental shelf, southern Bering Sea. *Marine Geology*, *35*(4), 299–329. https://doi.org/10.1016/0025-3227(80)90123-1

Gordeev, V. V., Beeskow, B., & Rachold, V. (2007). Geochemistry of the Ob and Yenisey estuaries: A comparative study. *Berichte zur Polar-und Meeresforschung* (Vol. 565, 235 pp.). Germany: AWI-Bremerhaven.

Gordeev, V. V., Rachold, V., & Vlasova, I. E. (2004). Geochemical behaviour of major and trace elements in suspended particulate material of the Irtysh river, the main tributary of the Ob river, Siberia. *Applied Geochemistry*, *19*(4), 593–610. https://doi.org/10.1016/j.apgeochem.2003.08.004

Hamilton, T. D. (1986). Late Cenozoic glaciation of the central Brooks Range. In T. D. Hamilton, K. M. Reed, & R. M. Thorson (Eds.), *Glaciation in Alaska; The geologic record*, (pp. 9–49). Anchorage: Alaska Geological Society.

Hanslik, D., Jakobsson, M., Backman, J., Björck, S., Sellén, E., O'Regan, M., et al. (2010). Quaternary Arctic Ocean sea ice variations and radiocarbon reservoir age corrections. *Quaternary Science Reviews*, *29*(25-26), 3430–3441. https://doi.org/10.1016/j.quascirev.2010.06.011

Harrison, J. C., St-Onge, M. R., Petrov, O. V., Strelnikov, S. I., Lopatin, B. G., Wilson, F. H., et al. (2011). Geological map of the Arctic. Geological Survey of Canada Open File, 5816.

Héquette, A., Marie-Hélène, R., & Hill, P. R. (1995). The effects of the Holocene sea level rise on the evolution of the southeastern coast of the Canadian Beaufort Sea. *Journal of Coastal Research*, *11*, 494–507.

Hill, J. C., & Driscoll, N. W. (2008). Paleodrainage on the Chukchi shelf reveals sea level history and meltwater discharge. *Marine Geology*, *254*(3-4), 129–151. https://doi.org/10.1016/j.margeo.2008.05.018

Hill, J. C., & Driscoll, N. W. (2010). Iceberg discharge to the Chukchi shelf during the Younger Dryas. *Quaternary Research*, *74*(1), 57–62. https://doi.org/10.1016/j.yqres.2010.03.008

Hillaire-Marcel, C., Maccali, J., Not, C., & Poirier, A. (2013). Geochemical and isotopic tracers of Arctic Sea ice sources and export with special attention to the Younger Dryas interval. *Quaternary Science Reviews*, *79*, 184–190. https://doi.org/10.1016/j.quascirev.2013.05.001

Holemann, J. A., Schirmacher, M., Kassens, H., & Prange, A. (1999). Geochemistry of surficial and ice-rafted sediments from the Laptev Sea (Siberia). *Estuarine, Coastal and Shelf Science*, *49*(1), 45–59. https://doi.org/10.1006/ecss.1999.0485

Jakobsson, M., Pearce, C., Cronin, T. M., Backman, J., Anderson, L. G., Barrientos, N., et al. (2017). Post-glacial flooding of the Beringia Land Bridge dated to 11,000 cal yrs BP based on new geophysical and sediment records. *Climate of the Past Discussions*, *13*, 991–1005. https://doi.org/10.5194/cp-13-991-2017

Jombart, T. (2008). Adegenet: A R package for the multivariate analysis of genetic markers. *Bioinformatics*, *24*(11), 1403–1405. https://doi.org/10.1093/bioinformatics/btn129

Kalinenko, V. V. (2001). Clay minerals in sediments of the Arctic seas. *Lithology and Mineral Resources*, *36*(4), 362–372. https://doi.org/10.1023/A:1010414305264

Keigwin, L. D., Donnelly, J. P., Cook, M. S., Driscoll, N. W., & Brigham-Grette, J. (2006). Rapid sea-level rise and Holocene climate in the Chukchi Sea. *Geology*, *34*(10), 861–864. https://doi.org/10.1130/G22712.1

Khim, B. K., Lee, M. J., Cho, H. G., & Park, K. (2018). Surface water productivity and sediment transport by Bering Strait throughflow in the Chukchi Shelf (the western Arctic Ocean) during the Holocene. *Holocene*, *28*, 814–826. https://doi.org/10.1177/0959683617744265

Kobayashi, D., Yamamoto, M., Irino, T., Nam, S.-I., Park, Y.-H., Harada, N., et al. (2016). Distribution of detrital minerals and sediment color in western Arctic Ocean and northern Bering Sea sediments: Changes in the provenance of western Arctic Ocean sediments since the last glacial period. *Polar Science*, *10*(4), 519–531. https://doi.org/10.1016/j.polar.2016.07.005

Krumm, S. (2006). SediCalc (free geological software).

Krylov, A. A., Stein, R., & Ermakova, L. A. (2014). Clay minerals as indicators of late quaternary sedimentation constraints in the Mendeleev Rise, Amerasian Basin, Arctic Ocean. *Lithology and Mineral Resources*, *49*(1), 103–116. https://doi.org/10.1134/S0024490213060059

Lakeman, T. R., Pie, A. J., Nixon, F. C., Furze, M. F. A., Blasco, S., Andrews, J. T., & King, E. L. (2018). Collapse of a marine-based ice stream during the early Younger Dryas chronozone, western Canadian Arctic. *46*, 1–4. https://doi.org/10.1130/G39665.1

Lambeck, K., Rouby, H., Purcell, A., Sun, Y., & Sambridge, M. (2014). Sea level and global ice volumes from the Last Glacial Maximum to the Holocene. *Proceedings of the National Academy of Sciences of the United States of America*, *111*, 15,296–15,303. https://doi.org/10.1073/pnas.1411762111

Lisé-Pronovost, A., St-Onge, G., Brachfeld, S., Barletta, F., & Darby, D. (2009). Paleomagnetic constraints on the Holocene stratigraphy of the Arctic Alaskan margin. *Global and Planetary Change*, *68*(1-2), 85–99. https://doi.org/10.1016/j.gloplacha.2009.03.015

Maccali, J., Hillaire-Marcel, C., Carignan, J., & Reisberg, L. C. (2013). Geochemical signatures of sediments documenting Arctic sea-ice and water mass export through Fram Strait since the Last Glacial Maximum. *Quaternary Science Reviews*, *64*, 136–151. https://doi.org/10.1016/j.quascirev.2012.10.029

McKay, J. L., de Vernal, A., Hillaire-Marcel, C., Not, C., Polyak, L., & Darby, D. (2008). Holocene fluctuations in Arctic sea-ice cover: Dinocyst-based reconstructions for the eastern Chukchi Sea. *Canadian Journal of Earth Sciences*, *45*(11), 1377–1397. https://doi.org/10.1139/E08-046

McNeely, R., Dyke, A. S., & Southon, J. R. (2006). Canadian marine reservoir ages, preliminary data assessment, Open File 5049.3, 3. https://doi.org/10.13140/2.1.1461.6649

Millot, R., Gaillardet, J., Dupré, B., & Allégre, C. J. (2003). Northern latitude chemical weathering rates: Clues from the Mackenzie River Basin, Canada. *Geochimica et Cosmochimica Acta*, *67*(7), 1305–1329. https://doi.org/10.1016/S0016-7037(02)01207-3

Montero-Serrano, J. C., Deschamps, C.-E., & Jaegle, M. (2014). Amundsen expedition report: Geology and paleoceanography Leg 2a. ArctiNet, Université Laval.
Murton, J. B., Bateman, M. D., Dallimore, S. R., Teller, J. T., & Yang, Z. (2010). Identification of Younger Dryas outburst flood path from Lake Agassiz to the Arctic Ocean. *Nature*, *464*, 740–743. https://doi.org/10.1038/nature08954
Naidu, A. S., Burrell, D. C., & Hood, D. W. (1971). Clay mineral composition and geological significance of some Beaufort Sea sediments. *Journal of Sedimentary Petrology*, *41*, 691–694. https://doi.org/10.1306/74D72329-2B21-11D7-8648000102C1865D
Naidu, A. S., Creager, J. S., & Mowatt, T. C. (1982). Clay mineral dispersal patterns in the north Bering and Chukchi Seas. *Marine Geology*, *47*(1-2), 1–15. https://doi.org/10.1016/0025-3227(82)90016-0
Naidu, A. S., & Mowatt, T. C. (1983). Sources and dispersal patterns of clay minerals in surface sediments from the continental-shelf areas off Alaska. *Geological Society of America Bulletin*, *94*(7), 841–854. https://doi.org/10.1130/0016-7606(1983)94
Not, C., & Hillaire-Marcel, C. (2012). Enhanced sea-ice export from the Arctic during the Younger Dryas. *Nature Communications*, *3*(1), 647–647. https://doi.org/10.1016/j.marchem.2011.12.005
Ortiz, J. D., Polyak, L., Grebmeier, J. M., Darby, D., Eberl, D. D., Naidu, S., & Nof, D. (2009). Provenance of Holocene sediment on the Chukchi-Alaskan margin based on combined diffuse spectral reflectance and quantitative X-ray diffraction analysis. *Global and Planetary Change*, *68*(1-2), 73–84. https://doi.org/10.1016/j.gloplacha.2009.03.020
Osterberg, E. C., Mayewski, P. A., Fisher, D. A., Kreutz, K. J., Maasch, K. A., Sneed, S. B., & Kelsey, E. (2014). Mount Logan ice core record of tropical and solar influences on Aleutian low variability: 500–1998 A.D. *Journal of Geophysical Research: Atmospheres*, *119*, 11,189–111,204. https://doi.org/10.1002/2014JD021847
Overland, J. E., Adams, J. M., Bond, N. A., Climate, J. O. F., Marine, P., Overland, J. E., et al. (1999). Decadal variability of the Aleutian low and its relation to high-latitude circulation. *Journal of Climate*, *12*(5), 1542–1548. https://doi.org/10.1175/1520-0442(1999)012
Padgham, W. A., & Fyson, W. K. (1992). The Slave Province: A distinct Archean craton. *Canadian Journal of Earth Sciences*, *29*(10), 2072–2086. https://doi.org/10.1139/e92-165
Petschick, R. (2000). MacDiff 4.2.5 manual. Germany: Institut für Geologie, Universität Erlangen.
Phillips, R. L., & Grantz, A. (2001). Regional variations in provenance and abundance of ice-rafted clasts in Arctic Ocean sediments: Implications for the configuration of late Quaternary oceanic and atmospheric circulation in the Arctic. *Marine Geology*, *172*(1-2), 91–115. https://doi.org/10.1016/S0025-3227(00)00101-8
Pickart, R. S. (2004). Shelfbreak circulation in the Alaskan Beaufort Sea: Mean structure and variability. *Journal of Geophysical Research*, *109*, C04024. https://doi.org/10.1029/2003JC001912
Polyak, L., Belt, S. T., Cabedo-Sanz, P., Yamamoto, M., & Park, Y. H. (2016). Holocene sea-ice conditions and circulation at the Chukchi-Alaskan margin, Arctic Ocean, inferred from biomarker proxies. *The Holocene*, *26*(11), 1810–1821. https://doi.org/10.1177/0959683616645939
Polyak, L., Darby, D. A., Bischof, J. F., & Jakobsson, M. (2007). Stratigraphic constraints on late Pleistocene glacial erosion and deglaciation of the Chukchi margin, Arctic Ocean. *Quaternary Research*, *67*(2), 234–245. https://doi.org/10.1016/j.yqres.2006.08.001
Pourmand, A., Dauphas, N., & Ireland, T. J. (2012). A novel extraction chromatography and MC-ICP-MS technique for rapid analysis of REE, Sc and Y: Revising CI-chondrite and post-Archean Australian Shale (PAAS) abundances. *Chemical Geology*, *291*, 38–54. https://doi.org/10.1016/j.chemgeo.2011.08.011
Rachold, V. (1999). Major, trace, and rare earth element geochemistry of suspended particulate material of East Siberian rivers draining to the Arctic Ocean. In Springer (Ed.), *Land-ocean systems in the Siberian Arctic: Dynamics and history*, (pp. 199–222). Berlin: Springer.
Rachold, V., Alabyan, a., Hubberten, H. W., Korotaev, V. N., & Zaitsev, A. A. (1996). Sediment transport to the Laptev Sea—Hydrology and geochemistry of the Lena River. *Polar Research*, *15*(2), 183–196. https://doi.org/10.1111/j.1751-8369.1996.tb00468.x
Reimer, P. J., Bard, E., Bayliss, A., Beck, J. W., Blackwell, P. G., Ramsey, C. B., et al. (2013). IntCal13 and Marine13 radiocarbon age calibration curves 0–50,000 years cal BP. *Radiocarbon*, *55*, 1869–1887. https://doi.org/10.2458/azu_js_rc.55.16947
Savenko, V. S., Pokrovskii, O. S., Dupre, B., & Baturin, N. (2004). Chemical composition of the suspended matter of Russia and adjacent countries. *Doklady Earth Sciences*, *238*, 938–942.
Schoster, F., Behrends, M., Muller, R., Stein, R., & Washner, M. (2000). Modern river discharge and pathways of supplied material in the Eurasian Arctic Ocean: Evidence from mineral assemblages and major and minor element distribution. *International Journal of Earth Sciences*, *89*(3), 486–495. https://doi.org/10.1007/s005310000120
Scott, D. B., Schell, T., St-Onge, G., Rochon, A., & Blasco, S. (2009). Foraminiferal assemblage changes over the last 15,000 years on the Mackenzie-Beaufort sea slope and Amundsen Gulf, Canada: Implications for past sea ice conditions. *Paleoceanography*, *24*, PA2219. https://doi.org/10.1029/2007PA001575
Stein, R., Fahl, K., Schade, I., Manerung, A., Wassmuth, S., Niessen, F., & Nam, S.-I. (2017). Holocene variability in sea ice cover, primary production, and Pacific-Water inflow and climate change in the Chukchi and East Siberian Seas (Arctic Ocean). *Journal of Quaternary Science*, *32*(3), 362–379. https://doi.org/10.1002/jqs.2929
Stokes, C. R., Clark, C. D., Darby, D. A., & Hodgson, D. A. (2005). Late Pleistocene ice export events into the Arctic Ocean from the M'Clure Strait Ice Stream, Canadian Arctic Archipelago. *Global and Planetary Change*, *49*(3-4), 139–162. https://doi.org/10.1016/j.gloplacha.2005.06.001
Stokes, C. R., Clark, C. D., & Storrar, R. (2009). Major changes in ice stream dynamics during deglaciation of the north-western margin of the Laurentide Ice Sheet. *Quaternary Science Reviews*, *28*(7-8), 721–738. https://doi.org/10.1016/j.quascirev.2008.07.019
Stokes, C. R., Clark, C. D., & Winsborrow, C. M. (2006). Subglacial bedform evidence for a major palaeo-ice stream and its retreat phases in Amundsen Gulf, Canadian Arctic Archipelago. *Journal of Quaternary Science*, *21*(4), 399–412. https://doi.org/10.1002/jqs.991
Tarasov, L., & Peltier, W. R. (2005). Arctic freshwater forcing of the Younger Dryas cold reversal. *Nature*, *435*(7042), 662–665. https://doi.org/10.1038/nature03617
Thió-Henestrosa, S., & Martín-Fernández, J. A. (2005). Dealing with compositional data: The freeware CoDaPack. *Mathematical Geology*, *37*(7), 773–793. https://doi.org/10.1007/s11004-005-7379-3
Tremblay, L. B., Mysak, L. A., & Dyke, A. S. (1997). Evidence from driftwood records for century-to-millennial scale variations of the high latitude atmospheric circulation during the Holocene. *Geophysical Research Letters*, *24*(16), 2027–2030. https://doi.org/10.1029/97GL02028
Trenberth, K. E., & Hurrell, J. W. (1994). Decadal atmospheric-ocean variations in the Pacific. *Climate Dynamics*, *9*(6), 303–319. https://doi.org/10.1007/BF00204745
van den Boogaart, K. G., & Tolosana-Delgado, R. (2008). "Compositions": A unified R package to analyze compositional data. *Computers and Geosciences*, *34*(4), 320–338. https://doi.org/10.1016/j.cageo.2006.11.017
van den Boogaart, K. G., & Tolosana-Delgado, R. (2013). Analyzing compositional data with R. (273 pp.). Heidelberg-New York-Dodrecht-London: Springer. https://doi.org/10.1007/978-3-642-36809-7
Viscosi-Shirley, C., Mammone, K., Pisias, N., & Dymond, J. (2003). Clay mineralogy and multi-element chemistry of surface sediments on the Siberian-Arctic shelf: Implications for sediment provenance and grain size sorting. *Continental Shelf Research*, *23*(11-13), 1175–1200. https://doi.org/10.1016/S0278-4343(03)00091-8

Viscosi-Shirley, C., Pisias, N., & Mammone, K. (2003). Sediment source strength, transport pathways and accumulation patterns on the Siberian-Arctic's Chukchi and Laptev shelves. *Continental Shelf Research*, *23*(11-13), 1201–1225. https://doi.org/10.1016/S0278-4343(03)00090-6

Vogt, C. (1997). Regional and temporal variations of mineral assemblages in Arctic Ocean sediments as climatic indicator during glacial/interglacial changes. *Reports on Polar Research*, *251*(1), 309.

von Eynatten, H., Tolosana-Delgado, R., & Karius, V. (2012). Sediment generation in modern glacial settings: Grain-size and source-rock control on sediment composition. *Sedimentary Geology*, *280*, 80–92. https://doi.org/10.1016/j.sedgeo.2012.03.008

Wagner, A., Lohmann, G., & Prange, M. (2011). Arctic river discharge trends since 7 ka BP. *Global and Planetary Change*, *79*(1-2), 48–60. https://doi.org/10.1016/j.gloplacha.2011.07.006

Wahsner, M., Müller, C., Stein, R., Ivanov, G., Levitan, M., Shelekhova, E., & Tarasov, G. (1999). Clay-mineral distribution in surface sediments of the Eurasian Arctic Ocean and continental margin as indicator for source areas and transport pathways—A synthesis. *Boreas*, *28*(1), 215–233. https://doi.org/10.1111/j.1502-3885.1999.tb00216.x

Weingartner, T., Aagaard, K., Woodgate, R., Danielson, S., Sasaki, Y., & Cavalieri, D. (2005). Circulation on the north central Chukchi Sea shelf. *Deep Sea Research Part II: Topical Studies in Oceanography*, *52*(24-26), 3175–3198. https://doi.org/10.1016/j.dsr2.2005.10.009

Weltje, G. J. (1997). End-member modeling of compositional data: Numerical-statistical algorithms for solving the explicit mixing problem. *Mathematical Geology*, *29*(4), 503–549. https://doi.org/10.1007/BF02775085

Wickert, A. D. (2016). Reconstruction of North American drainage basins and river discharge since the Last Glacial Maximum. *Earth Surface Dynamics*, *4*(4), 831–869. https://doi.org/10.5194/esurf-4-831-2016

Yamamoto, M., Nam, S.-I., Polyak, L., Kobayashi, D., Suzuki, K., Irino, T., & Shimada, K. (2017). Holocene dynamics in the Bering Strait inflow to the Arctic and the Beaufort Gyre circulation based on sedimentary records from the Chukchi Sea. *Climate of the Past*, *13*(9), 1111–1127. https://doi.org/10.5194/cp-13-1111-2017

Erratum

In the originally published version of this article, an incorrect version of the supporting information file was posted. The file has since been corrected and this version may be considered the authoritative version of record.